Theoret. Comput. Fluid Dynamics (1996) 8: 105–129

Theoretical and Computational Fluid Dynamics

The Hydrodynamic Stability of Channel Flow with Compliant Boundaries[1]

J.S.B. Gajjar and P. Sibanda

Department of Mathematics, University of Manchester,
Oxford Road, Manchester M13 9PL, England

Communicated by Philip Hall

Received 1 December 1994 and accepted 9 February 1995

Abstract. An asymptotic theory is developed for the hydrodynamic stability of an incompressible fluid flowing in a channel in which one wall is rigid and the other is compliant. We exploit the multideck structure of the flow to investigate theoretically the development of disturbances to the flow in the limit of large Reynolds numbers. A simple spring-plate model is used to describe the motion of the compliant wall, and this study considers the effect of the various wall parameters, such as tension, inertia, and damping, on the stability properties. An amplitude equation for a modulated wavetrain is derived and the properties of this equation are studied for a number of cases including linear and nonlinear theory. It is shown that in general the effect of viscoelastic damping is destabilizing. In particular, for large damping, the analysis points to a fast travelling wave, short-scale instability, which may be related to a flutter instability observed in some experiments. This work also demonstrates that the conclusions obtained by previous investigators in which the effect of tension, inertia, and other parameters is neglected, may be misleading. Finally it is shown that a set of compliant-wall parameters exists for which the Haberman type of critical layer analysis leads to stable equilibrium amplitudes, in contrast to many other stability problems where such equilibrium amplitudes are unstable.

1. Introduction

The first major theoretical investigation into the effects of a flexible boundary on the hydrodynamic stability of a boundary-layer flow was made by Benjamin (1960). His analysis, based on linear stability theory, showed *inter alia* that for flow over flexible surfaces three modes of instability could be excited. The first of these is similar to Tollmien–Schlichting instability but now modified by the effects of the flexible wall. These Class A waves are stabilized by a nondissipative flexible wall while internal damping has a destabilizing effect on this type of instability. The second type of unstable waves, or Class B waves, can exist with an inviscid fluid flow and depend solely on surface flexibility. The third form of instability, or Class C waves, are exited when the flexibility of the wall is large and are of the Kelvin–Helmholtz type. In a later study, Benjamin (1963) gave a more precise classification of the instabilities which, for inviscid flow over a compliant surface, were described by means of a generalized Lagrangian method. Further studies were made by Landahl (1962) who also confirmed Benjamin's findings about the destabilizing nature of internal damping on Class A instabilities.

[1] P.S. is grateful to the University of Zimbabwe for financial support. J.S.B.G. is grateful to the E.P.S.R.C. for the computing resources acquired under Grants GR/H58568-C88 and GR/H 83683 used in this research.

Building on the work of Landahl, Gyorgyfalvy (1967) carried out an extensive analytical study of the stability and transition of boundary layers over flexible surfaces. He found that a flexible surface can significantly reduce the amplification rates of Class A instabilities leading to a delay in the onset of transition to turbulence. In an earlier study of parallel shear flow over a general compliant surface, Landahl and Kaplan (1965) had also shown that a careful choice of the compliant surface properties can lead to a significant reduction of the spatial amplification rates. It was also generally accepted that to achieve any appreciable delay in transition it would be necessary to use a light and highly flexible membrane. Recent work by Carpenter and Garrad (1985) has cast doubt on these conclusions for "Kramer-type" compliant surfaces.

The model investigated by Carpenter and Garrad (1986) is a "Kramer-type" compliant surface. Their approach admits both approximate theory and a numerical scheme to solve the Orr–Sommerfeld equation. Following Landahl (1962), the objective was to determine the effects of any change in the mechanical properties of the compliant coating on the hydrodynamic stability of the flow. Their study concentrated on Class A waves, the Tollmien–Schlichting instability (TSI). Class B waves, also called flow-induced surface in stabilities (FISI) were considered in a later study, see Carpenter and Garrad (1986). The main conclusion, later confirmed by Willis (1986) is that any effects which stabilize the TSI will inevitably destabilize the FISI.

A review of some of the earlier experimental and theoretical work involving compliant surfaces is given in Bushnell *et al.* (1977). More recent research on compliant flows is extensively reviewed in the articles by Riley *et al.* (1988) and Carpenter (1990).

In this paper we are particularly interested in determining the effects of a flexible boundary on the hydrodynamic stability of plane Poiseuille flow. Extensive studies of plane channel flow with rigid walls have been made by, among others, Reid (1965), Smith (1979), and Gajjar and Smith (1985). Early investigations of the flow in a channel with compliant boundaries were made by Hains and Price (1962). In their numerical studies both channel surfaces were assumed to be stretched flexible membranes. The neutral stability curves obtained for this problem were compared with the rigid-wall model and the main effect of the flexibility was to form a closed stability curve reducing the region of instability to between known upper and lower critical Reynolds numbers.

More recent work has been reported by Rotenberry (1992). He also assumed that both walls were compliant and used a streamfunction formulation to calculate the travelling-wave solutions that bifurcate from plane Poiseuille flow along a neutral stability curve in the Reynolds number, wave number plane. Despite suggestions that transition is modified in flow over compliant boundaries, see Rotenberry and Saffman (1990), he concluded that for finite amplitude disturbances, transition for the flow over compliant walls is qualitatively similar to that for rigid boundaries. In a recent study, Ehrenstein and Rossi (1993) considered the problem of channel flow with one compliant surface. They used a streamfunction–vorticity formulation to compute nonlinear neutral travelling-wave solutions.

The problem of a channel flow with flexible walls is of considerable interest in certain medical applications, particularly in relation to the phenomenon of wheezing for people suffering from lung or bronchial disorders. In this respect Grotberg and Reiss (1984) and Grotberg and Shee (1985) have investigated the stability of uniform plug flow in a channel with two flexible boundaries. See also Grotberg and Davies (1980), and the more general review on lung and cardiovascular flows by Grotberg (1994). In Grotberg and Shee (1985) and Grotberg and Reiss (1984) the viscous terms are approximated by a simpler model involving a friction factor multiplying the velocity, and both papers concentrate solely on the inviscid linear and nonlinear stability of the travelling-wave flutter mode. Some comparisons with experimental data (Gavriely *et al.*, 1984, 1989) show encouraging trends in certain areas.

It should be noted that the multiplicity of modes and the complex nature of the compliant material often means that a detailed mathematical analysis of compliant flows is impracticable. In the numerical studies the profusion of parameters makes a complete analysis rather difficult and to make the problem mathematically tractable a judicious choice of parameters and numerous simplifications have to be made. Despite these limitations, useful solutions can still be obtained from these studies.

In this study we consider the stability of channel flow with one compliant wall. This work has several objectives. One of the aims is to obtain quantitative as well as qualitative information, from a rational analytical viewpoint, of the effect on flow stability of the different wall parameters. For instance a question which is of some interest is how the TSI is modified by wall compliance and what set of parameters causes

the major departure from the rigid-wall solutions. Another objective is to study the nonlinear stability of the flow over compliant surfaces and to obtain an analytical description of the equilibrium surfaces which have been computed numerically by others. The analysis presented here enables a more systematic evaluation of the variation of the nonlinear neutral stability properties with different wall parameters. Whilst the major assumption used in the work below is that the Reynolds number is large, nevertheless as many other studies of this type have demonstrated, useful information can be obtained concerning the important scales and thin regions which govern the overall stability properties. This can give an invaluable guide for finite Reynolds number computations of such flows.

We exploit the multideck structure of the flow regime in the limit of large Reynolds number to make an asymptotic analysis of the perturbed flow. This technique has proven extremely valuable and accurate in similar studies of boundary-layer flows, see, for example, Carpenter and Gajjar (1990). In this paper we concentrate on upper-branch stability properties since these can then be used to predict the relevant scales for the travelling-wave flutter modes, see also Carpenter and Gajjar (1990). It is also possible to deduce the high frequency limit of the lower-branch modes using upper-branch scalings as in Wu *et al.* (1996). We derive simple formulae for the wave number and wave speed in both linear and nonlinear theories and compare these with similar expressions for the rigid-wall model. These expressions give a better insight into the quantitative and qualitative influence of the lower compliant surface on the hydrodynamic stability of the channel flow. The paper is organized as follows. Section 2 contains a linear analysis of the flow in the lower half of the channel. It consists of three subsections; in Section 2.1 the basic theory is given and an asymptotic analysis developed for the lower flow regions. The compliant-wall model considered in the paper is given in Section 2.2, while Section 2.3 gives an analysis of the Stokes wall layer. In Section 3 we consider the upper half of the channel and match the solutions across the whole channel. Section 4 contains a nonlinear analysis of the critical layer. Some implications of the theory and the results are discussed in Section 5 and we finally give a summary of our findings in Section 6.

1.1 Problem Formulation

The fundamental problem considered here is the theoretical model of an incompressible fluid flowing in a channel with a lower compliant boundary. We consider long waves and assume that the Reynolds number is large. The governing nondimensional unsteady Navier–Stokes equations for an incompressible fluid in two dimensions are as follows:

$$\begin{aligned}
&\frac{\partial u}{\partial x}+\frac{\partial v}{\partial y}=0,\\
&\frac{\partial u}{\partial t}+u\frac{\partial u}{\partial x}+v\frac{\partial u}{\partial y}=-\frac{\partial p}{\partial x}+\frac{1}{R}\left(\frac{\partial^2 u}{\partial x^2}+\frac{\partial^2 u}{\partial y^2}\right),\\
&\frac{\partial v}{\partial t}+u\frac{\partial v}{\partial x}+v\frac{\partial v}{\partial y}=-\frac{\partial p}{\partial y}+\frac{1}{R}\left(\frac{\partial^2 v}{\partial x^2}+\frac{\partial^2 v}{\partial y^2}\right).
\end{aligned} \tag{1.1}$$

Equations (1.1) have been nondimensionalized such that the space coordinates are given by $(x', y') = L(x, y)$, the velocity components by $(u', v') = U(u, v)$, the pressure by $p' = \rho_* U^2 p$, the density by $\rho' = \rho_* \rho$, and the time by $t' = (L/U)t$. We take L to be the undisturbed channel width, U to be the centreline speed, and define a channel-flow Reynolds number based on L by $R = UL/\nu_*$, where ν_* is the coefficient of kinematic viscosity of the fluid.

In nondimensional terms the upper channel wall is located at $y = 1$, while the compliant wall is located at $y = \eta(x, t)$. The undisturbed flow is given by the velocity $(U_B, 0)$ where $U_B(y) = y(1 - y)$. In the analysis below however we work with a more general profile $U_B(y)$ with the properties

$$U_B \sim \lambda_1 y + \lambda_2 y^2 + \cdots \qquad \text{as} \quad y \to 0.$$

The coefficients $\lambda_1 = dU_B/dy(0) > 0$ and $\lambda_2 = d^2U_B/dy^2(0) < 0$ are respectively the skin friction and the curvature of the basic flow profile. For the lower wall we assume a simple plate membrane model so that the change in the mechanical fluid pressure Δp due to the displacement of the lower surface, η, is

related to the flow quantities through the relation (Carpenter and Garrad, 1985; Rotenberry, 1992)

$$\Delta p = \frac{T}{R^2}\frac{\partial^2 \eta}{\partial x^2} - M\frac{\partial^2 \eta}{\partial t^2} - \frac{d}{R}\frac{\partial \eta}{\partial t} - \frac{B}{R^2}\frac{\partial^4 \eta}{\partial x^4} - \frac{\kappa \eta}{R^2}. \tag{1.2}$$

Here the quantities M, d, B, T, and κ are respectively the mass density per unit length, the damping, the flexural rigidity of the plate, the tension, and the spring stiffness. Equation (1.2) has been nondimensionalized using the fluid density ρ, the channel width L, the centreline velocity U, and the viscosity μ where $\eta = \hat{\eta}/L, \Delta p = \Delta \hat{p}/\rho U^2, T = \hat{T}\rho L/\mu^2, \kappa = \hat{\kappa} L^3 \rho/\mu^2, M = \rho_B \hat{b}/\rho L, d = \hat{d}L/\mu$, and $B = \hat{B}\rho\mu^2 L$. We have imposed the constant pressure gradient condition and chosen $U = L^2 p/8\mu$ to be the characteristic velocity of the parabolic velocity profile with p the mean pressure gradient.

The boundary condition on the velocity is

$$u = 0, \qquad v = \frac{\partial \eta}{\partial t} \qquad \text{when} \quad y = \eta(x,t). \tag{1.3}$$

At the upper rigid channel wall, the no-slip condition holds so that

$$u = v = 0 \qquad \text{at} \quad y = +1.$$

The compliant-wall equation (1.2) gives the condition for the dynamic pressure at the flexible surface. The compliancy of the lower channel wall removes any imposition of symmetry on the solution of the problem.

The asymptotic structure for the upper-branch stability of channel flows is now well known and is given, for example, in Smith (1979). The neutral wave number and phase speed are of $O(\varepsilon)$, and $O(\varepsilon^2)$, respectively, where $\varepsilon = R^{-1/11}$ ($\ll 1$). We thus set $\alpha = \varepsilon\alpha_0$ and $c = \varepsilon^2 c_0$, respectively, where α_0, c_0 are the scaled real wave number and real phase speed, respectively, of the travelling-wave disturbance. The disturbances are taken to be in the form of a modulated wavetrain, periodic in X and dependent on additional slow scale X_1,

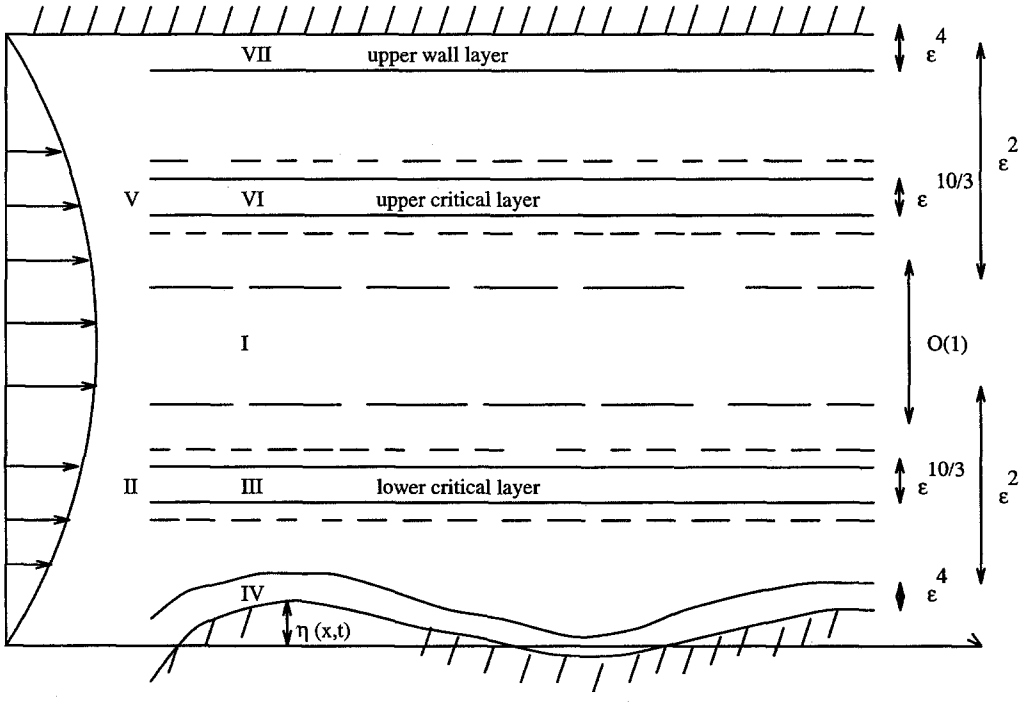

Figure 1. A schematic representation of the disturbance structure for channel flow.

T_1 so that

$$\frac{\partial}{\partial x} = \varepsilon\alpha_0 \frac{\partial}{\partial X} + \varepsilon^3 \frac{\partial}{\partial X_1}, \tag{1.4}$$

$$\frac{\partial}{\partial t} = -\varepsilon^3 c_0 \alpha_0 \frac{\partial}{\partial X} + \varepsilon^5 \frac{\partial}{\partial T_1}. \tag{1.5}$$

A further discussion of the scalings used here may be found in Gajjar and Smith (1985). We introduce small disturbances to the basic channel flow of size $\delta \ll 1$. We also assume in each region, a solution in the form of an asymptotic series expansion in terms of the scale factor ε for the disturbance velocity and pressure quantities. The disturbance structure consists of several zones, I–VII, governing the development of the flow. A schematic diagram of the flow structure is shown in Figure 1. The central region I is a passive shear layer where $y = O(1)$. Regions II and V contain the two critical layers, regions III and VI respectively, and are both $O(\varepsilon^2)$ while regions III and VI are of $O(\varepsilon^{10/3})$. The flow regions IV and VII are the viscous wall layers at the flexible surface and the rigid wall, respectively, and are of $O(\varepsilon^4)$. Additional diffusion layers embedded in regions II and V, astride the critical layer, which are necessary because of the properties of the unsteady critical layer, will be introduced in Section 4.

2. Disturbance Expansions

2.1. Outer Flow Region

Following Gajjar and Smith (1985) the first significant departure from linear theory occurs when the disturbance size δ is of $O(R^{-14/33})$. Below we work with a disturbance size δ which is taken to be of $O(R^{-14/33})$. We chose to work with the expansions in terms of δ and ε as this facilitates a direct comparison with linear theory. Linear theory may then be recovered by taking δ to be infinitesimally small. Below we consider each of the regions in turn and write down appropriate expansions of the disturbance quantities. Since the analysis is similar to that for the rigid-wall case only the details necessary to obtain the nonlinear dispersion relations are given. Most of the governing equations of the disturbance quantities may be deduced from earlier work such as Smith (1979) and Gajjar and Smith (1985).

In the central region I the flow is given by the expansions

$$u = U_B + \delta\tilde{u}_0 + \delta\varepsilon^2\tilde{u}_1 + \cdots, \tag{2.1a}$$

$$v = \delta\varepsilon\tilde{v}_0 + \delta\varepsilon^3\tilde{v}_1 + \cdots, \tag{2.1b}$$

$$p = p_B + \delta\varepsilon^2\tilde{p}_0 + \delta\varepsilon^4\tilde{p}_1 + \cdots. \tag{2.1c}$$

Substituting (2.1) into the Navier–Stokes equations gives a sequence of equations for the disturbance quantities which can be solved to give

$$\tilde{u}_0 = AU_{By}, \tag{2.2a}$$

$$\tilde{v}_0 = -\alpha_0 A_X U_B, \tag{2.2b}$$

$$\tilde{p}_0 = P_0 - \alpha_0^2 A \int_0^y U_B^2 dy. \tag{2.2c}$$

Here $A = A(X, X_1, T_1)$ and $P_0(X, X_1, T_1)$ are unknown functions representing the disturbance displacement and pressure amplitude at the lower wall, and we write $A = \bar{A}(X_1, T_1)e^{iX} + \text{c.c.}$ and $P_0 = \bar{P}(X_1, T_1)e^{iX} + \text{c.c.}$ (where c.c. denotes the complex conjugate).

At the next order we obtain the solutions

$$\tilde{v}_1 = \alpha_0 U_B \int_{1/2}^{y} \frac{\tilde{p}_{0X}}{U_B^2}\, dy + \alpha_0 c_0 A_X - \alpha_0 A_{1X} U_B, \tag{2.3a}$$

$$\tilde{u}_1 = -U_{By} \int_{1/2}^{y} \frac{\tilde{p}_0}{U_B^2}\, dy - \frac{\tilde{p}_0}{U_B} - \frac{A_1 U_{By}}{i\alpha_0} - \frac{A_{X_1} U_{B_y}}{i\alpha_0}, \tag{2.3b}$$

$$\tilde{p}_1 = P_1 + \alpha_0^2 \int_0^y U_B^2 \left(\int_{1/2}^{y} \frac{\tilde{p}_0}{U_B^2}\, dy \right) dy + 2\alpha_0^2 c_0 A \int_0^y U_B\, dy + \alpha_0^2 A_{1XX} \int_0^y U_B^2\, dy + \alpha_0 A_{XX_1} \int_0^y U_B^2\, dy, \tag{2.3c}$$

where the additional displacement A_1 and the pressure P_1 are unknown functions of X, X_1, T_1. The integrals in (2.3a,b) have a logarithmic singularity at $y = 0$ (and also at $y = 1$) which becomes more apparent in the study of region II and the critical layer. In region II containing the critical layer, the appropriate scaled transverse coordinate is related to y by $y = \varepsilon^2 \bar{Y}$ with $\bar{Y} \sim O(1)$.

Introducing this, along with the preceding results and the solutions in region I, we have the following expansions:

$$u = \lambda_1 \varepsilon^2 \bar{Y} + \lambda_2 \varepsilon^4 \bar{Y}^2 + \cdots + \delta(\bar{u}_0 + \varepsilon^2 \bar{u}_1) + \cdots, \tag{2.4a}$$

$$v = \delta\varepsilon(\varepsilon^2 \bar{v}_0 + \varepsilon^4 \bar{v}_1 + \cdots), \tag{2.4b}$$

$$p = p_B + \delta(\varepsilon^2 \bar{p}_0 + \varepsilon^4 \bar{p}_1 + \cdots), \tag{2.4c}$$

$$\eta = \delta(\eta_0 + \varepsilon^2 \eta_1 + \cdots), \tag{2.4d}$$

where $\lambda_1 = U_{By}|_{y=0}$ and $2\lambda_2 = U_{Byy}|_{y=0}$. Thus substituting the above equations into (1.1) we obtain the solutions

$$\bar{v}_0 = -\alpha_0 \frac{\bar{p}_{0X}}{\lambda_1} - \alpha_0 A_X(\lambda_1 \bar{Y} - c_0), \tag{2.5a}$$

$$\bar{u}_0 = \lambda_1 A, \tag{2.5b}$$

$$\bar{p}_0 = P_0(X, X_1, T_1). \tag{2.5c}$$

Setting $\bar{Y} = 0$ in (2.5a) and using the boundary condition (1.3) gives

$$\bar{p}_0 = P_0 = c_0 \lambda_1 (A + \eta_0). \tag{2.6}$$

At the next order we obtain

$$\bar{v}_1 = -\frac{1}{\lambda_1}[\alpha_0 \bar{p}_{1X} + \bar{p}_{0X_1} + \lambda_1(A_{T_1} + c_0 A_{X_1})] - \alpha_0 \lambda_2 A_X \left(\xi^2 + 2\frac{c_0}{\lambda_1} \xi\{\ln|\xi| + \varphi^{\pm}\} - \frac{c_0^2}{\lambda_1^2} \right)$$
$$- 2\alpha_0 c_0 \frac{\lambda_2}{\lambda_1} \eta_{0X} \left(\xi\{\ln|\xi| + \varphi^{\pm}\} - \frac{c_0}{\lambda_1} \right) - \bar{A}_{1X} \alpha_0 \lambda_1 \xi, \tag{2.7a}$$

$$\bar{u}_1 = \lambda_2 A \left(2\xi + 2\frac{c_0}{\lambda_1}[1 + \ln|\xi| + \varphi^{\pm}] \right) + 2c_0 \frac{\lambda_2}{\lambda_1} \eta_0 (1 + \ln|\xi| + \varphi^{\pm}) + \bar{A}_1 \lambda_1 - \frac{\lambda_1}{i\alpha_0} A_{X_1}, \tag{2.7b}$$

$$\bar{p}_1 = P_1, \tag{2.7c}$$

where $\bar{A}_1$ is an unknown function of X, X_1, T_1, and $\xi = (\bar{Y} - c_0/\lambda_1)$. These solutions contain terms which are irregular when $\bar{Y} = c_0/\lambda_1$ and a critical layer of thickness $O(\varepsilon^{10/3})$ has to be introduced to smooth out these singularities. The terms $\varphi^{\pm}$ are introduced to connect the solutions either side of the critical layer (the $+$ sign refers to ξ positive and the $-$ sign to ξ negative). In linear theory it is well known that $(\varphi^+ - \varphi^-)$ is equal to $i\pi$.

Before considering the wall layer it is convenient to return to the motion of the compliant wall.

2.2. The Compliant-Wall Model

Equation (1.2) is written as

$$\Delta p = p' = \bar{T}\eta_{xx} - M_s \varepsilon^{-4} \eta_{tt} - \bar{d}\varepsilon\eta_t - B_s \eta_{xxxx} - \kappa_s \eta. \tag{2.8}$$

Here η is the small vertical displacement of the lower surface and the constants $\bar{T}, M_s, B_s, \bar{d}$, and κ_s are related to the original parameters by

$$\kappa_s = \frac{\kappa\varepsilon^{-2}}{R^2}, \qquad B_s = \frac{B\varepsilon^2}{R^2}, \qquad M_s = M\varepsilon^4, \qquad \bar{T} = \frac{T}{R}, \qquad \bar{d} = \frac{d\varepsilon^{-1}}{R}.$$

This choice of scaling enables the scaled parameters to appear as $O(1)$ constants in the eigenvalue relation and therefore allows a greater range of compliant properties to be studied. By taking appropriate limits the structure for other cases can be deduced from the analysis below. The fluctuating pressure at the wall is given by p' and by expanding p', η in the form

$$p' = \delta(\varepsilon^2 \hat{p}_0 + \varepsilon^4 \hat{p}_1 + \cdots),$$
$$\eta = \delta(\eta_0 + \varepsilon^2 \eta_1 + \cdots),$$

we obtain, using (2.8), (2.2c), (2.3c),

$$\hat{p}_0 = P_0 = s_0 \eta_0, \qquad \text{where} \quad s_0 = -\bar{T}\alpha_0^2 + M_s \alpha_0^2 c_0^2 - B_s \alpha_0^4 - \kappa_s, \tag{2.9}$$

where we have taken $\eta_0 = \hat{\eta}_0(X_1, T_1)e^{ix} + \text{c.c.}$ At the next order we obtain

$$\hat{p}_1 = P_1 = \mathscr{L}\eta_1 + 2\alpha_0 \bar{T}\eta_{0XX_1} + \bar{d}\alpha_0 c_0 \eta_{0X} + 2M_s \alpha_0 c_0 \eta_{0XT_1} + 4B_s \alpha_0^3 \eta_{0XX_1}, \tag{2.10}$$

where the operator $\mathscr{L}$ is defined by

$$\mathscr{L}\eta = \alpha_0^2 \bar{T}\eta_{XX} - M_s \alpha_0^2 c_0^2 \eta_{XX} - B_s \alpha_0^4 \eta_{XXXX} - \kappa_s \eta.$$

2.3. The Stokes Layer

In the Stokes layer, of $O(\varepsilon^4)$, region IV in Figure 1, the analysis deviates significantly from that given for the main channel and the adjoining flow regions. In this region Z is an $O(1)$ coordinate where

$$y = \eta(x, t) + \varepsilon^4 Z,$$

and we introduce the Prandtl transformation so that the expansions then take the form

$$u = U_B + \delta\hat{u}_0 + \cdots, \tag{2.11a}$$
$$v = \eta_t(x, t) + \delta\varepsilon^5 \hat{v}_0 + \cdots, \tag{2.11b}$$
$$p = p_B + \delta\varepsilon^2 \hat{p}_0 + \cdots. \tag{2.11c}$$

The leading-order equations which govern the Stokes-layer flow are a linear system of partial differential equations,

$$\alpha_0 \frac{\partial \hat{u}_0}{\partial X} + \frac{\partial \hat{v}_0}{\partial Z} = 0, \tag{2.12a}$$

$$-\alpha_0 c_0 \left(\frac{\partial \hat{u}_0}{\partial X} + \lambda_1 \frac{\partial \eta_0}{\partial X} \right) = -\alpha_0 \frac{\partial \hat{p}_0}{\partial X} + \frac{\partial^2 \hat{u}}{\partial Z^2}, \tag{2.12b}$$

$$\hat{p}_0 = s_0 \eta_0, \tag{2.12c}$$

with boundary conditions

$$\hat{u}_0 \sim \lambda_1 A \qquad \text{as} \quad Z \to \infty, \tag{2.13a}$$
$$\hat{u}_0 = -\lambda_1 \eta_0 \qquad \text{at} \quad Z = 0, \tag{2.13b}$$
$$\hat{v}_0 = 0 \qquad \text{at} \quad Z = 0, \tag{2.13c}$$

to match with the solution in region II and satisfy the conditions at the flexible wall. Solving (2.12) with the above boundary conditions gives

$$\hat{u}_0 = \frac{\hat{p}_0}{c_0} - \frac{\hat{p}_0}{c_0} e^{-mZ} - \lambda_1 \eta, \tag{2.14}$$

where

$$m = (\alpha_0 c_0)^{1/2} e^{-i(\pi/4)}.$$

Thus using (2.12a) we obtain,

$$\hat{v}_0 = -i\alpha_0 \left(\frac{\hat{p}_0}{c_0} - \lambda_1 \eta \right) Z - i\alpha_0 \frac{\hat{p}_0}{mc_0} (e^{-mZ} - 1). \tag{2.15}$$

Of interest in the derivation of the amplitude equation is the displacement from the wall layer which is given by the finite part of $\hat{v}_0$, $\hat{v}_{0f}$, say, as $Z \to \infty$ and from (2.15) we see that

$$\hat{v}_{0f} = i \frac{\alpha_0 \hat{p}_0}{mc_0}.$$

2.4. The Upper Regions of the Channel

Regions V–VII in the upper half of the channel wall are analogous with the corresponding regions II–IV in the lower half of the channel, but with the compliant surface replaced by a rigid wall. The important results may therefore be deduced from the analysis given in the earlier sections.

In region V, which contains the upper critical layer, with $y = 1 + \varepsilon^2 \tilde{Y}$, the expansions follow from (2.1) and the solutions in flow region I in particular:

$$u = \hat{\lambda}_1 \varepsilon^2 \tilde{Y} + \hat{\lambda}_2 \varepsilon^4 \tilde{Y}^2 + \delta(\tilde{u}_0 + \varepsilon^2 \tilde{u}_1 + \cdots), \tag{2.16a}$$

$$v = \delta\varepsilon(\varepsilon^2 \tilde{v}_0 + \varepsilon^4 \tilde{v}_1 + \cdots), \tag{2.16b}$$

$$p = p_B + \delta(\varepsilon^2 \tilde{p}_0 + \varepsilon^4 \tilde{p}_1 + \cdots). \tag{2.16c}$$

The following results are obtained for the leading-order problem:

$$\tilde{u}_0 = \hat{\lambda}_1 A, \qquad \tilde{v}_0 = -\alpha_0 \hat{\lambda}_1 A_X \tilde{Y}, \quad \text{and} \quad \tilde{p}_0 = c_0 \hat{\lambda}_1 A, \tag{2.17}$$

where the constants $\hat{\lambda}_1$ and $\hat{\lambda}_2$ are given by

$$\hat{\lambda}_1 = U_{By}|_{y=1}, \qquad 2\hat{\lambda}_2 = U_{Byy}|_{y=1}. \tag{2.18}$$

The second-order problem is solved to obtain

$$\tilde{v}_1 = -\frac{1}{\hat{\lambda}_1}[\alpha_0 \tilde{p}_{1X} + \tilde{p}_{0X_1} + \lambda_1 (A_{T_1} + c_0 A_{X_1})] - \alpha_0 \hat{\lambda}_2 A_X \left(\tilde{\xi}^2 + 2\frac{c_0}{\hat{\lambda}_1} \tilde{\xi}[\ln|\tilde{\xi}| + \tilde{\varphi}^{\pm}] - \frac{c_0^2}{\hat{\lambda}_1} \right) - \tilde{A}_{1X} \alpha_0 \hat{\lambda}_1 \xi, \tag{2.19a}$$

$$\tilde{p}_1 = \tilde{p}_1(X, X_1, T_1), \tag{2.19b}$$

where $\tilde{\xi} = \tilde{Y} - (c_0/\hat{\lambda}_1)$ and the functions $\tilde{\varphi}^{\pm}$ arise from the continuation across the upper critical layer (the + sign refers to $\tilde{\xi}$ positive and the − sign to $\tilde{\xi}$ negative).

The analysis of the Stokes layer at the upper rigid wall is similar to that near the lower wall, and it is found that the displacement condition on $\tilde{v}_1$ is given by

$$\tilde{\tilde{v}}_1(\tilde{Y} = 0) = -i \frac{\alpha_0 \tilde{\tilde{p}}_0}{c_0 m}.$$

Before analysing the critical layers and the diffusion layers, it is convenient at this stage to derive the amplitude equation for the evolution of the disturbance. This is obtained by matching the various flow quantities across the different regions. The role of the critical layers here is relatively passive in the sense that the normalized critical-layer equations are of Haberman (1972) type with unsteadiness (in X_1, T_1) appearing in parametric form. This is very different from problems in which the full unsteady nonlinear critical-layer equations arise, and where the interaction and coupling with development of the amplitude is much stronger. The diffusion layers here exist to smooth out the large mean flow jumps produced by the Haberman critical layer.

3. Eigenrelations and Derivation of the Amplitude Equation

Firstly if we consider regions I and II$^+$, the matching of the normal velocities using (2.2b), (2.3a), (2.5), (2.7a) leads to the relation

$$D_0 A_X - \alpha_0 \lambda_1 A_{1X} = -\frac{2c_0\lambda_2\alpha_0}{\lambda_1}(A_X + \eta_{0X})\varphi^+ - \alpha_0\lambda_1\bar{A}_{1X}, \tag{3.1}$$

where D_0 (and the other D_i's below) are real constants which are given in Appendix A.

Next matching the normal velocities between regions II$^-$ and the Stokes layer, region V, shows that

$$-\frac{1}{\lambda_1}[\alpha_0\bar{p}_{1X} + \bar{p}_{0X_1} + \lambda_1(A_{T_1} + c_0 A_{X_1})] + \frac{2\lambda_2\alpha_0 c_0^2}{\lambda_1^2}(A_X + \eta_{0X})\varphi^- + c_0\alpha_0\bar{A}_{1X} + A_X D_1 = \frac{i\alpha_0\hat{p}_0}{mc_0} + \eta_{0T_1} - \alpha_0 c_0\eta_{1X}. \tag{3.2}$$

Similarly matching the normal velocities in the regions in the upper half of the channel leads to

$$-\alpha_0\hat{\lambda}_1\tilde{A}_{1X} - \frac{2\hat{\lambda}_2 c_0\alpha_0}{\hat{\lambda}_1}A_X\tilde{\varphi}^- = D_2 A_X - \alpha_0\hat{\lambda}_1 A_{1X} \tag{3.3}$$

and

$$-\frac{1}{\hat{\lambda}_1}[\alpha_0\tilde{\bar{p}}_{1X} + \tilde{\bar{p}}_{0X_1} + \hat{\lambda}_1(A_{T_1} + c_0 A_{X_1})] + \frac{2\hat{\lambda}_2\alpha_0 c_0^2}{\hat{\lambda}_1^2}A_X\left(\varphi^+ + \ln\left|\frac{c_0}{\hat{\lambda}_1}\right|\right) + c_0\alpha_0\tilde{A}_{1X} = \frac{i\alpha_0\tilde{\bar{p}}_0}{c_0 m}. \tag{3.4}$$

Next matching the pressures between regions I, II, and IV shows that

$$\bar{p}_0 = P_0 = \hat{p}_0, \qquad \bar{p}_1 = P_1 = \hat{p}_1. \tag{3.5}$$

The pressures in the lower and upper half of the channel may be matched to give

$$\tilde{\bar{p}}_0 = P_0 - \alpha_0^2 A I_0 \tag{3.6}$$

and

$$\tilde{\bar{p}}_1 = P_1 + 2c_0\alpha_0^2 A I_1 + \alpha_0 I_0 A_{XX_1} + P_0\alpha_0^2 I_2 - \alpha_0^4 A I_3 + \alpha_0^2 A_{1XX} I_0, \tag{3.7}$$

where

$$I_0 = \int_0^1 U_B^2\, dy,$$

and the other integrals in (3.7) are defined in Appendix A.

The relations (2.6), (2.9), (2.17), (3.5), and (3.6) may be combined to yield

$$c_0^2\lambda_1\hat{\lambda}_1 - c_0 s_0(\hat{\lambda}_1 - \lambda_1) = \alpha_0^2 I_0(s_0 - c_0\lambda_1), \tag{3.8}$$

which is the dispersion relation fixing the wave number to the phase speed.

Relations (3.1)–(3.8) above may be used to eliminate P_1, $\bar{A}_1$, η_1, $\tilde{A}_1$, $\tilde{\bar{p}}_0$, and $\tilde{\bar{p}}_1$ to obtain an expression which determines the higher-harmonic components of A_1 (and therefore some of the other quantities). If we restrict attention to the e^{iX} components, then after some algebra (3.1)–(3.8) lead to

$$\begin{aligned}
&iA_0(c_0 D_0 - \lambda_1 D_1) - i\alpha_0 c_0\lambda_1 A_{11} + \frac{i\alpha_0\lambda_1\hat{p}_0}{mc_0} + \lambda_1\eta_{0T_1} \\
&\quad + \frac{\alpha_0 c_0\lambda_1}{s_0}[-2\alpha_0\bar{T}\eta_{0X_1} - \bar{d}\alpha_0 c_0\eta_0 - 2M_s\alpha_0 c_0\eta_{0T_1} - 4B_s\alpha_0^3\eta_{0X1}] \\
&= -\frac{2c_0^2\lambda_2\alpha_0 i}{\lambda_1}(A + \eta_0)(\varphi^+ - \varphi^-) - p_{0X_1} - \lambda_1(A_{T_1} + c_0 A_{X_1}) - \left(1 - \frac{c_0\lambda_1}{s_0}\right) \\
&\quad \times\left[\frac{2i\hat{\lambda}_2}{\hat{\lambda}_1}\alpha_0 c_0^2 A(\tilde{\varphi}^+ - \tilde{\varphi}^-) + \alpha_0^2 A_{X_1} I_0 + i\alpha_0(I_0\alpha_0^2 + \hat{\lambda}_1 c_0)A_{11} - (\tilde{\bar{p}}_{0X_1} + \hat{\lambda}_1(A_{T1} + c_0 A_{X_1})) - iD_3 A + i\frac{\alpha_0\hat{\lambda}_1\tilde{\bar{p}}_0}{mc_0}\right],
\end{aligned} \tag{3.9}$$

where A_{11} is the e^{iX} component of A_1. Note that the coefficient of A_{11} in (3.9) is

$$-i\alpha_0 c_0\lambda_1+\left(1-\frac{c_0\lambda_1}{s_0}\right)i\alpha_0(I_0\alpha_0^2+\hat{\lambda}_1 c_0)$$

which is zero because of the dispersion relation (3.8). The e^{iX} coefficients of the remaining terms give the amplitude equation which may then be expressed as

$$\frac{\partial\bar{A}}{\partial T_1}+c_g\frac{\partial\bar{A}}{\partial X_1}=\frac{1}{D_5}\left\{\left[iD_4+\frac{\alpha_0^2c_0^3\lambda_1^2\bar{d}}{s_0(s_0-\lambda_1c_0)}-i\frac{\alpha_0 s_0\lambda_1^2}{m(s_0-c_0\lambda_1)}-i\frac{(s_0-c_0\lambda_1)\alpha_0\hat{\lambda}_1^2}{s_0 m}\right]\bar{A}\right.$$
$$\left.-2c_0^2\alpha_0 i\bar{A}\left[\frac{\lambda_2 s_0}{\lambda_1(s_0-c_0\lambda_1)}(\varphi^+-\varphi^-)+\frac{(s_0-c_0\lambda_1)\hat{\lambda}_2}{s_0\hat{\lambda}_1}(\tilde{\varphi}^+-\tilde{\varphi}^-)\right]\right\}, \tag{3.10}$$

where $c_g=\partial(\alpha_0c_0)/\partial\alpha_0$ is the group velocity of the wave and D_4, D_5 are given in the appendix. Equation (3.10) is the key result of this paper and some of the properties of this equation are studied in a later section. As can be seen from (3.10) the nonlinear evolution of the amplitude is strongly dependent on the jumps $(\varphi^+-\varphi^-)$ and $(\tilde{\varphi}^+-\tilde{\varphi}^-)$ across the lower and upper critical layers. We consider next therefore the details of the critical layer.

4. The Nonlinear Critical Layer

For the critical-layer and diffusion-layer analysis it is necessary to restore the dependence of δ on ε and we set $\delta=\varepsilon^{14/3}$. In the lower critical layer $y=\varepsilon^2c_0/\lambda_1+\varepsilon^{10/3}\tilde{y}$ and the critical-layer solutions expand as

$$u=\varepsilon^2c_0+\varepsilon^{10/3}\lambda_1\tilde{y}+\varepsilon^4c_0^2\frac{\lambda_2}{\lambda_1^2}+\varepsilon^{14/3}\tilde{U}_0+\varepsilon^{16/3}\frac{2c_0\lambda_2}{\lambda_1}\tilde{y}+\varepsilon^{20/3}\tilde{U}_1+\cdots, \tag{4.1a}$$

$$v=\varepsilon^{23/3}\tilde{V}_{-1}+\varepsilon^{27/3}\tilde{V}_0+\varepsilon^{29/3}\tilde{V}_1+\varepsilon^{33/3}\tilde{V}_2+\cdots, \tag{4.1b}$$

$$p=p_B+\varepsilon^{20/3}\tilde{P}_0+\varepsilon^{26/3}\tilde{P}_1+\varepsilon^{28/3}\tilde{P}_2+\cdots. \tag{4.1c}$$

The main differences here and in earlier studies are in the expansions for the mean flow terms in (4.1a). For a steady nonlinear critical layer a mean flow term of order $O(\varepsilon^{16/3})$ is present in (4.1a) as well as outside the critical layer in (2.1) to enable a match with the mean vorticity jump produced by the critical layer. Here because of unsteady effects such terms are not necessary. The diffusion layer serves to restore the mean vorticity jump produced by the critical layer back to zero outside the critical layer.

After substitution into the Navier–Stokes equations the leading-order quantities are found to have simple solutions. At higher order it is found that the solution for $\tilde{U}_1$ with $\zeta_1=\tilde{U}_{1\tilde{y}}$ is governed by

$$\alpha_0\lambda_1\tilde{y}\zeta_{1X}+\tilde{V}_{-1}\zeta_{1\tilde{y}}-\zeta_{1\tilde{y}\tilde{y}}=0,\qquad \tilde{V}_{-1}=-\frac{\alpha_0P_{0X}}{\lambda_1}, \tag{4.2}$$

with boundary conditions

$$\tilde{U}_1\sim\lambda_2\tilde{y}^2+2P_0\frac{\lambda_2}{\lambda_1^2}(\ln|\tilde{y}|+\varphi^{\pm})+\tilde{U}^{\pm}(X,X_1,T_1)+\tilde{H}^{\pm}(X_1,T_1)\tilde{y}+\cdots\qquad\text{as}\quad\tilde{y}\to\pm\infty. \tag{4.3}$$

Here $U^{\pm}$ contains the higher harmonics in e^{iX}, with the fundamental being absorbed by the $\varphi^{\pm}$ terms, and the $\tilde{H}^{\pm}$ terms are necessary because of the properties of the critical layer.

Since X_1, T_1 appear only parameterically in (4.2), (4.3) it is convenient to reduce the equations to a more standard form. If we set $P_0=\{|\bar{P}_0(X_1,T_1)|e^{i(\theta(X_1,T_1)+X)}+\text{c.c.}\}$ (where θ is real) and

$$\zeta_1=2\lambda_2d_1\zeta^*,\qquad\tilde{y}=d_1Y^*,$$

with

$$d_1=\frac{\sqrt{2}|\bar{P}_0|^{1/2}}{|\lambda|},\qquad\theta+X=X^*,\qquad\gamma_c=\frac{|\lambda_1^3|}{2^{3/2}|\bar{P}_0|^{3/2}\alpha_0\lambda_1},$$

then (4.2), (4.3) reduce to

$$Y^*\zeta^*_{X^*} + \sin X^*\zeta^*_{Y^*} - \gamma_c\zeta^*_{Y^*Y^*} = 0, \tag{4.4a}$$

$$\zeta^* \to H^{\pm} + Y^* + \frac{\cos X^*}{Y^*} \qquad \text{as} \quad Y^* \to \pm\infty, \tag{4.4b}$$

with

$$\varphi(\gamma_c) = \varphi^+ - \varphi^- = \frac{1}{\pi}\int_{-\infty}^{*\infty}\int_0^{2\pi} \zeta^* e^{-iX^*}\, dX^*\, dY^* = 4\gamma_c(H^+ - H^-), \tag{4.4c}$$

$$\tilde{H}^{\pm} = 2\lambda_2 d_1 H^{\pm}.$$

A similar analysis of the upper critical layer shows that the same problem as (4.4a,b) is obtained but with γ replaced by $\hat{\gamma}_c$, where

$$\hat{\gamma}_c = \frac{|\hat{\lambda}_1^3|}{2^{3/2}|\tilde{p}_0|^{3/2}\alpha_0\hat{\lambda}_1}. \tag{4.5}$$

This implies that the $\tilde{\varphi}^+ - \tilde{\varphi}^-$ across the upper critical layer is given by

$$\tilde{\varphi} = \tilde{\varphi}^+ - \tilde{\varphi}^- = \varphi(\hat{\gamma}_c) = \varphi(\sigma\gamma_c), \tag{4.6a}$$

where

$$\sigma = \left|\frac{\lambda_1 s_0}{\hat{\lambda}_1(s_0 - c_0\lambda_1)}\right|^{3/2}\frac{\lambda_1}{\hat{\lambda}_1}. \tag{4.6b}$$

For fixed X_1, T_1 and hence $|\bar{P}_0|$, the problem (4.4) needs to be solved numerically to determine $\varphi^{\pm}$ as functions of γ_c. The solution of this problem is now established (see Haberman, 1972; Smith and Bodonyi, 1982), and it has the property that Real$(i\varphi) \to -\pi$ as $\gamma_c \to \infty$ and Real$(i\varphi) \to -\gamma_c C^{(1)}$ as $\gamma_c \to 0$, where $C^{(1)}$ is a constant ($C^{(1)} = 5.516$). Note that the jump across the upper critical layer is not the same as that across the lower critical layer. The numerical solution of (4.4) shows that $\varphi(\gamma_c)$ is an odd function of γ_c and hence, for the case $\hat{\lambda}_1 = -\lambda_1$ studied below, $\tilde{\varphi}(\gamma_c) = -\varphi(|\sigma|\gamma_c)$.

We consider next the diffusion layers with $y = \varepsilon^2(c_0/\lambda_1) + \varepsilon^3\bar{Z}$ either side of the lower critical layer. As has already been mentioned the role of the diffusion layers is to reduce the mean vorticity jump (the $(H^+ - H^-)$ term) to zero outside the critical layer. The scalings used below may be derived as in Gajjar (1996). We have the expansions for the velocities and pressures in the form

$$\begin{aligned}
u &= \varepsilon^2 c_0 + \varepsilon^3\lambda_1\bar{Z} + \varepsilon^4\frac{\lambda_2 c_0^2}{\lambda_1^2} + \varepsilon^{14/3}\bar{u}_0 + \varepsilon^5\frac{2c_0\bar{Z}\lambda_2}{\lambda_1} + \varepsilon^6\lambda_2\bar{Z}^2 + \varepsilon^{19/3}\bar{u}_1 + \varepsilon^{20/3}\bar{u}_2 + \varepsilon^7\bar{u}_3 + \varepsilon^{22/3}\bar{u}_4 + \cdots,\\
v &= \varepsilon^3(\varepsilon^{14/3}\bar{v}_{-1} + \varepsilon^{17/3}\bar{v}_1 + \varepsilon^{20/3}\bar{v}_2 + \varepsilon^{23/3}\bar{v}_3 + \varepsilon^{24/3}\bar{v}_4 + \varepsilon^{25/3}\bar{v}_5 + \cdots),\\
p &= \varepsilon^{20/3}\bar{p}_0 + \varepsilon^{26/3}\bar{p}_1 + \varepsilon^{28/3}\bar{p}_2 + \varepsilon^{29/3}\bar{p}_3 + \cdots.
\end{aligned} \tag{4.7}$$

The solutions for the leading-order terms are trivial and are readily deduced by expanding the outer solution in region II in terms of $\bar{Z}$. It is found that $\bar{u}_{1X} = 0$, $\bar{p}_0 = P_0$, and

$$\bar{\zeta}_2 = \bar{u}_{2\bar{z}} = \frac{2\lambda_2}{\alpha_0\lambda_1^2\bar{Z}}\bar{p}_0 + \bar{\zeta}_{2M}(X_1, T_1, \bar{Z}).$$

At the next order the equation for $\bar{u}_4$ shows that

$$\bar{u}_{1T_1} + c_0\bar{u}_{1X_1} - \bar{u}_{1\bar{Z}\bar{Z}} = -\langle\bar{v}_{-1}\bar{\zeta}_2\rangle, \qquad \bar{v}_{-1} = -\frac{\alpha_0\bar{p}_{0X}}{\lambda_1} \tag{4.8}$$

after averaging in X over one period and the notation $\langle\cdot\rangle$ denotes the average of the quantity inside the brackets. Hence $\bar{\zeta}_1 = \bar{u}_{1\bar{z}}$ satisfies the equation

$$\bar{\zeta}_{1T_1} + c_0\bar{\zeta}_{1X_1} + c_0\bar{\zeta}_{1X_1} - \bar{\zeta}_{1\bar{Z}\bar{Z}} = 0, \tag{4.9a}$$

with the conditions

$$\bar{\zeta}_1 = \tilde{H}^{\pm}(X_1, T_1) \qquad \text{at} \quad \bar{Z} = \pm 0. \tag{4.9b}$$

This equation and the boundary conditions are the same as those obtained by Brown *et al.* (1993). The equation may be solved using Fourier transforms to obtain

$$\bar{\zeta}_1(Z, X_1, T_1) = \frac{1}{c_0} \int_{-\infty}^{X_1} \frac{|Z|}{2\sqrt{\pi}} \tilde{H}^{\pm}\left(q, T_1 - \frac{(X_1 - q)}{c_0}\right) \frac{\exp(-Z^2/4(X_1 - q))}{(X_1 - q)^{3/2}}\, dq.$$

The $\pm$ sign refers to the diffusion layer above and below the critical layer, respectively. It can be seen that the mean vorticity diffuses to zero away from the critical layer for large $|Z|$.

5. Results and Discussion

5.1. Linear Neutral Results

The results for linear theory may be deduced from (3.10) by taking the jump φ equal to $i\pi$ and using (4.6a). If we restrict attention to the neutral case, then the real part of (3.10) together with (3.8), determine the linear neutral eigenrelations as

$$-\frac{\alpha_0 \lambda_1^2 s_0}{\sqrt{2\bar{m}}(s_0 - c_0\lambda_1)} - \frac{\alpha_0 \hat{\lambda}_1^2}{\sqrt{2\bar{m}}}\left(\frac{s_0 - c_0\lambda_1}{s_0}\right) - \frac{\alpha_0^2 c_0^3 \lambda_1 d_{1r}}{s_0(s_0 - c_0\lambda_1)} = \frac{2c_0^2\lambda_2\alpha_0 s_0 \pi}{\lambda_1(s_0 - c_0\lambda_1)} - \frac{(s_0 - c_0\lambda_1)2\hat{\lambda}_2\alpha_0 c_0^2\pi}{s_0\hat{\lambda}_1}, \tag{5.1a}$$

$$c_0^2\lambda_1\hat{\lambda}_1 - c_0 s_0(\hat{\lambda}_1 - \lambda_1) = \alpha_0^2 I_0(s_0 - c_0\lambda_1), \tag{5.1b}$$

and where

$$s_0 = -\bar{T}\alpha_0^2 + M_s\alpha_0^2 c_0^2 - B_s\alpha_0^4 - \kappa_s. \tag{5.1c}$$

In the above we have set d_{1r} to be the real part of $\bar{d}_1$. For a given set of wall parameters $\bar{T}$, M_s, B_s, κ_s, $\bar{d}_{1r}$, (5.1a–c) can be solved numerically to obtain the neutral wave numbers α_0 and wave speed c_0. In the numerical results described in this paper we used the basic profile given by $U_B = y(1-y)$ giving $\hat{\lambda}_1 = -\lambda_1 = -1$ and $\lambda_2 = \hat{\lambda}_2 = -1$. With this basic profile (5.1a) reduces to

$$-\frac{\alpha_0\lambda_1^2}{\sqrt{2\bar{m}}} - \frac{\alpha_0^2 c_0^3 \lambda_1^2 d_{1r}}{(s_0^2 + (s_0 - c_0\lambda_1)^2)} = \frac{2c_0^2\lambda_2\pi\alpha_0}{\lambda_1}. \tag{5.1d}$$

A complete parametric study involving the variation of all the parameters $\bar{T}$, M_s, B_s, κ_s, d_{1r}, in addition to the amplitude A, is beyond the scope of this paper. The results presented in Figures 2–10 are for a selected set of parameters, and the general trends shown in these figures for various limiting cases are confirmed by further analysis below.

In Figure 2(a)–(d) we show the variation of the neutral wave number α_0, and neutral phase speed c_0 for different values of damping, against κ_s with M_s, B_s, $\bar{T}$ set to zero. The most pronounced deviation from the rigid-wall results occurs for small values of κ_s and for large values of damping. For a fixed value of damping, as κ_s increases the rigid-wall results are recovered. For certain values of damping there are three roots of the dispersion curves, although these are connected, see, for example, Figures 2(b), (d) and 3(a), (b). In Figure 3 we show the variation of α_0 and c_0 against d_{1r} for $\kappa_s = 5$ with M_s, B_s, $\bar{T}$ set equal to zero. It is seen that as damping increases the rigid-wall solution disappears and is replaced by one with much larger wave numbers and enhanced wave speeds.

In Figure 4(a)–(d) we show some results for α_0, c_0 against the scaled tension parameter $\bar{T}$, for different values of damping. For fixed κ_s and d_{1r} the smaller values of tension produce significantly much larger wave numbers and wave speeds than the rigid-wall case. For large $\bar{T}$ the rigid-wall values are again recovered. In Figure 5(a), (b) we show the variation of α_0, c_0 against d_{1r} for fixed values of κ_s and $\bar{T}$. This again shows that

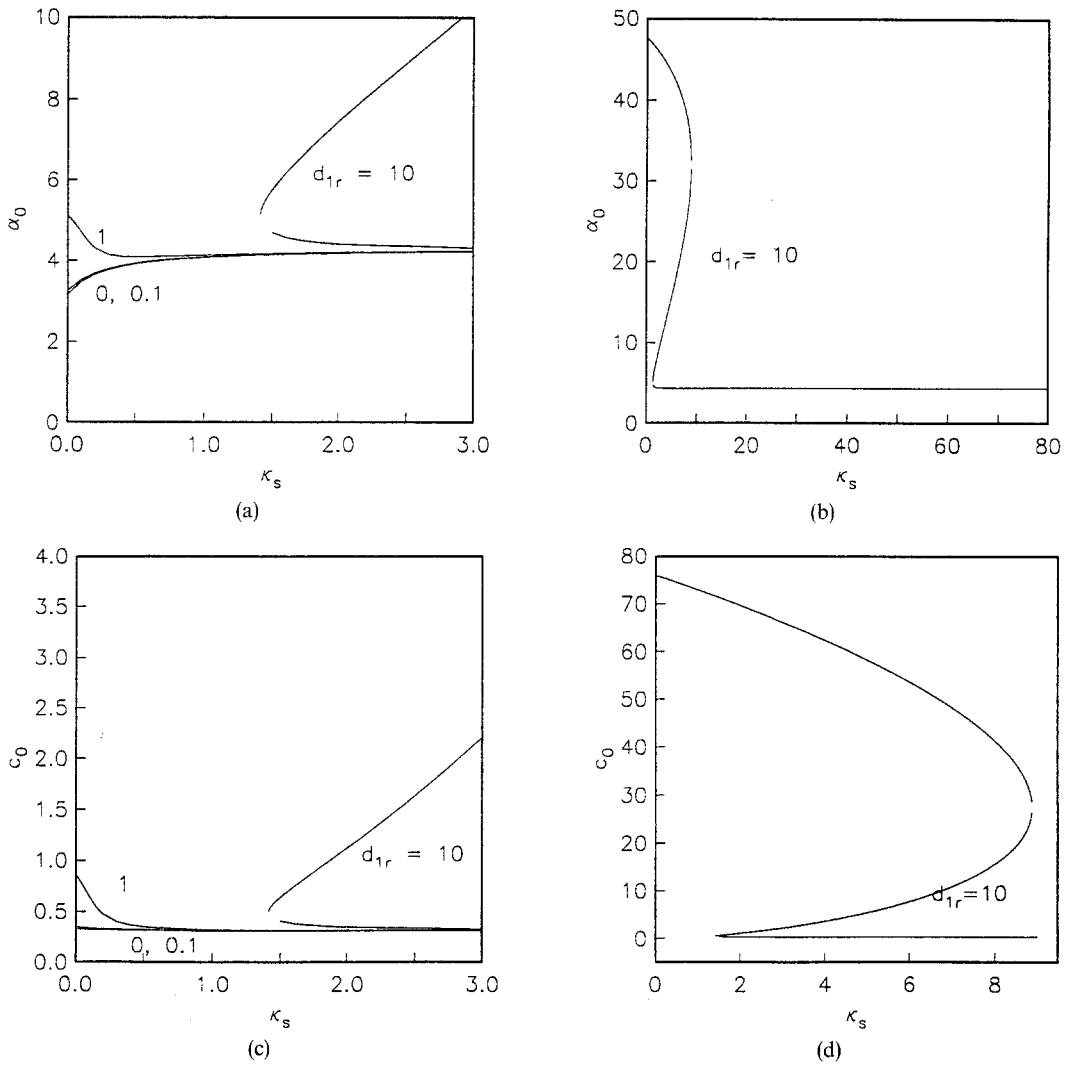

Figure 2. (a) Linear neutral wave number α_0 against κ_s for $d_{1r} = 0, 0.1, 1$, and 10. The values of M_s, B_s, and $\bar{T}$ are all zero. (b) Same as (a) for $d_{1r} = 10$ but shown on a different scale. (c) Neutral phase speeds c_0 against κ_s with the same values of the other parameters as in (a). (d) Same as (c) but for $d_{1r} = 10$ shown on a different scale.

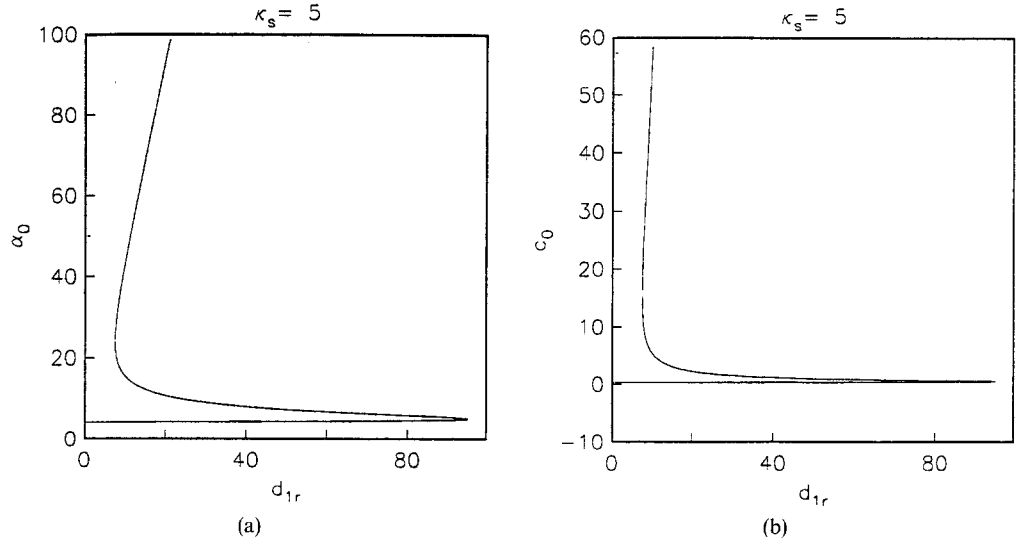

Figure 3. (a) Linear neutral wave number α_0 against scaled damping d_{1r}, with $\kappa_s = 5$ and $M_s = B_s = \bar{T} = 0$. (b) Same as (a) but with wave speed c_0.

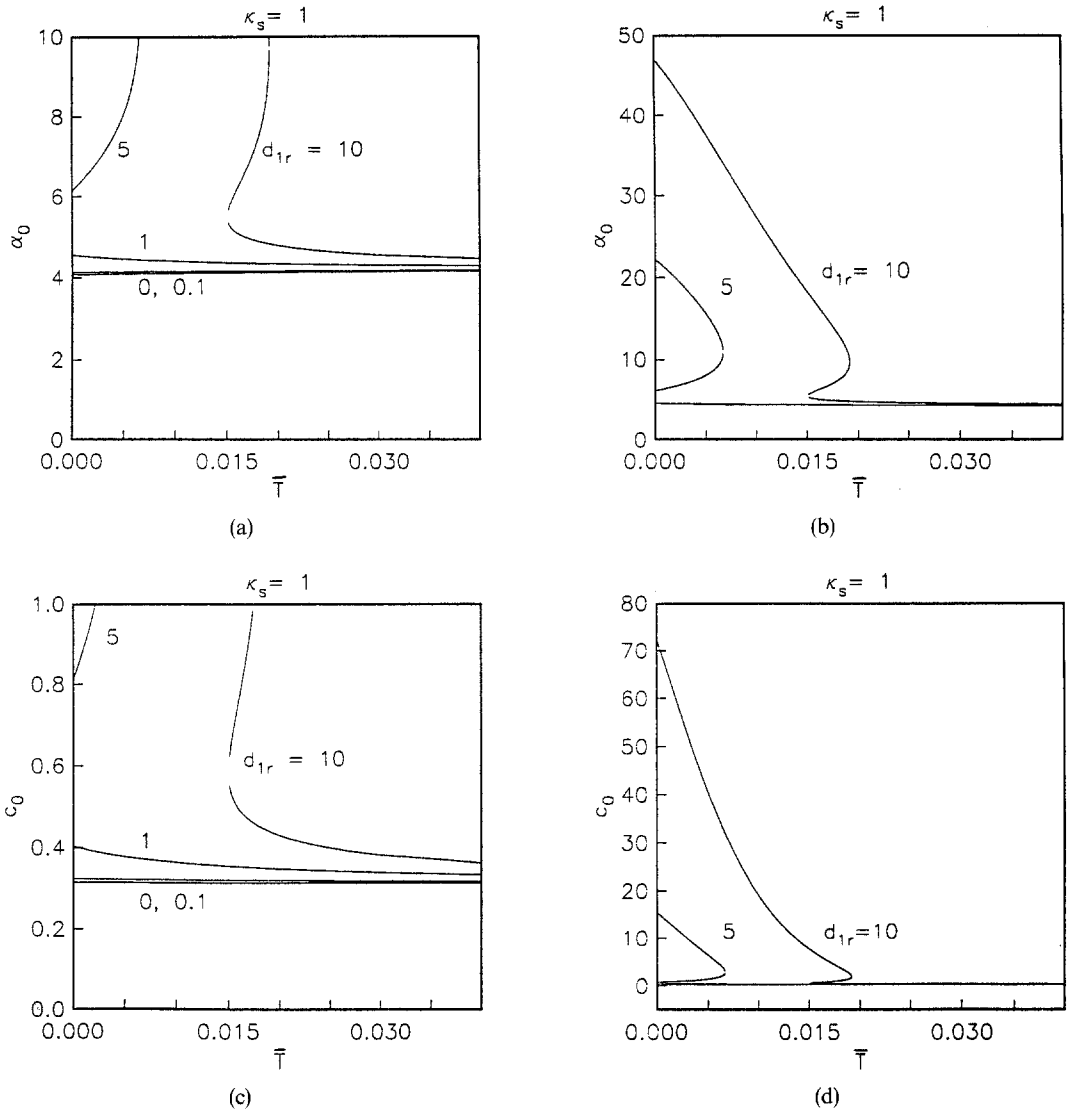

Figure 4. (a) Linear neutral α_0 against scaled tension $\bar{T}$ for different values of damping and with $\kappa_s = 1$ and $M_s = B_s = 0$. (b) Curves for $d_{1r} = 5$ and 10 shown on a different scale. (c) Same as (a) except for phase speed c_0. (d) Same as (c) but curves for $d_{1r} = 5$ and 10 shown on a different scale.

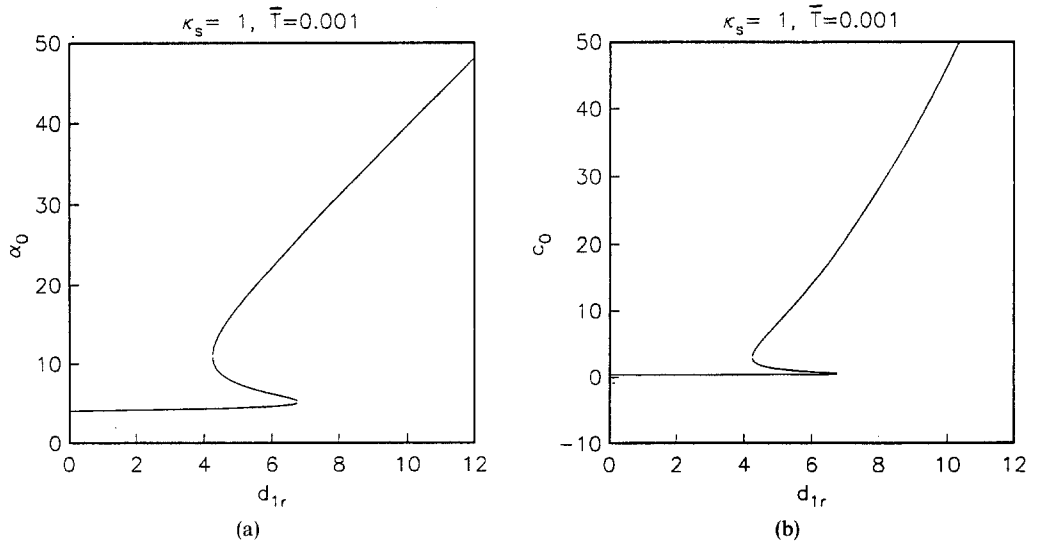

Figure 5. (a) Linear neutral α_0 and (b) c_0 against d_{1r} with $\kappa_s = 1$, $\bar{T} = 0.001$, and $M_s = B_s = 0$.

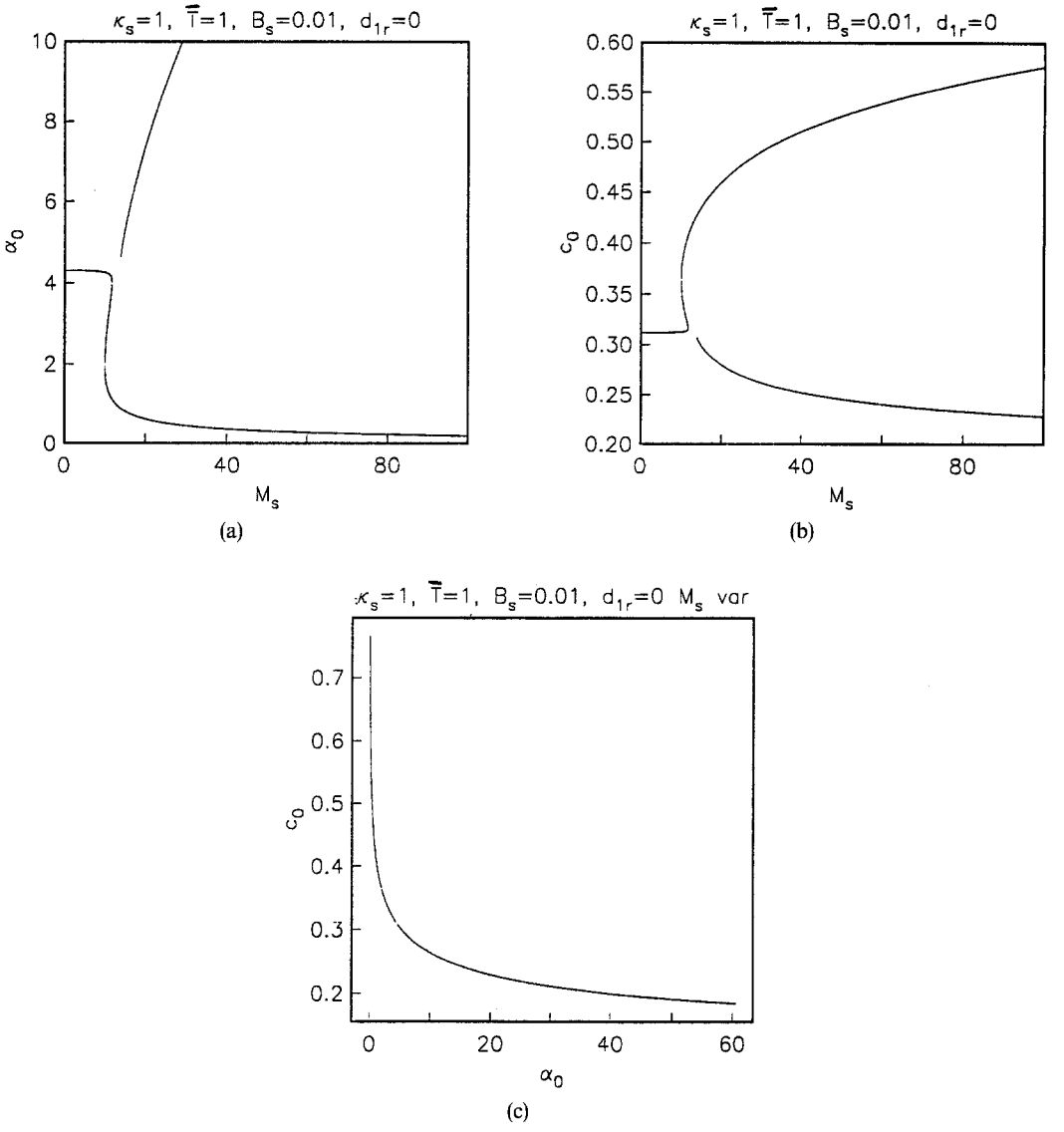

Figure 6. (a) Linear neutral α_0 against M_s with $\bar{T} = 1, B_s = 0.01, \kappa_s = 1$, and $d_{1r} = 0$. (b) Same as (a) but for phase speed c_0. (c) Variation of α_0 against c_0 with M_s varying, other parameters as in (a).

as damping increases, beyond a critical value of damping, three distinct roots of the dispersion relations exists. For larger damping the rigid-wall solution is again replaced by one with larger wave numbers and phase speeds.

In Figure 6(a)–(c) we show α_0 and c_0 against M_s for fixed values of the other parameters and zero damping. There are now four distinct roots and three join continuously to merge with the rigid-wall solution. The fourth root appears to be disjoint, and this suggests that for M_s nonzero there are two distinct modes. For large values of M_s one of the modes represents a fast travelling wave with small wave numbers, and the other mode is a much shorter slowly travelling wave.

In Figure 7(a)–(e) we show the variation of α_0 and c_0 against damping for nonzero values of the other parameters. Again for certain values of damping there are four roots to the dispersion relations. As damping increases two of the roots join continuously together and merge with the rigid-wall root. For very large damping there are only two roots and these represent two distinct modes. This is shown clearly in Figure 7(e) where we plot α_0 against c_0 with damping varying.

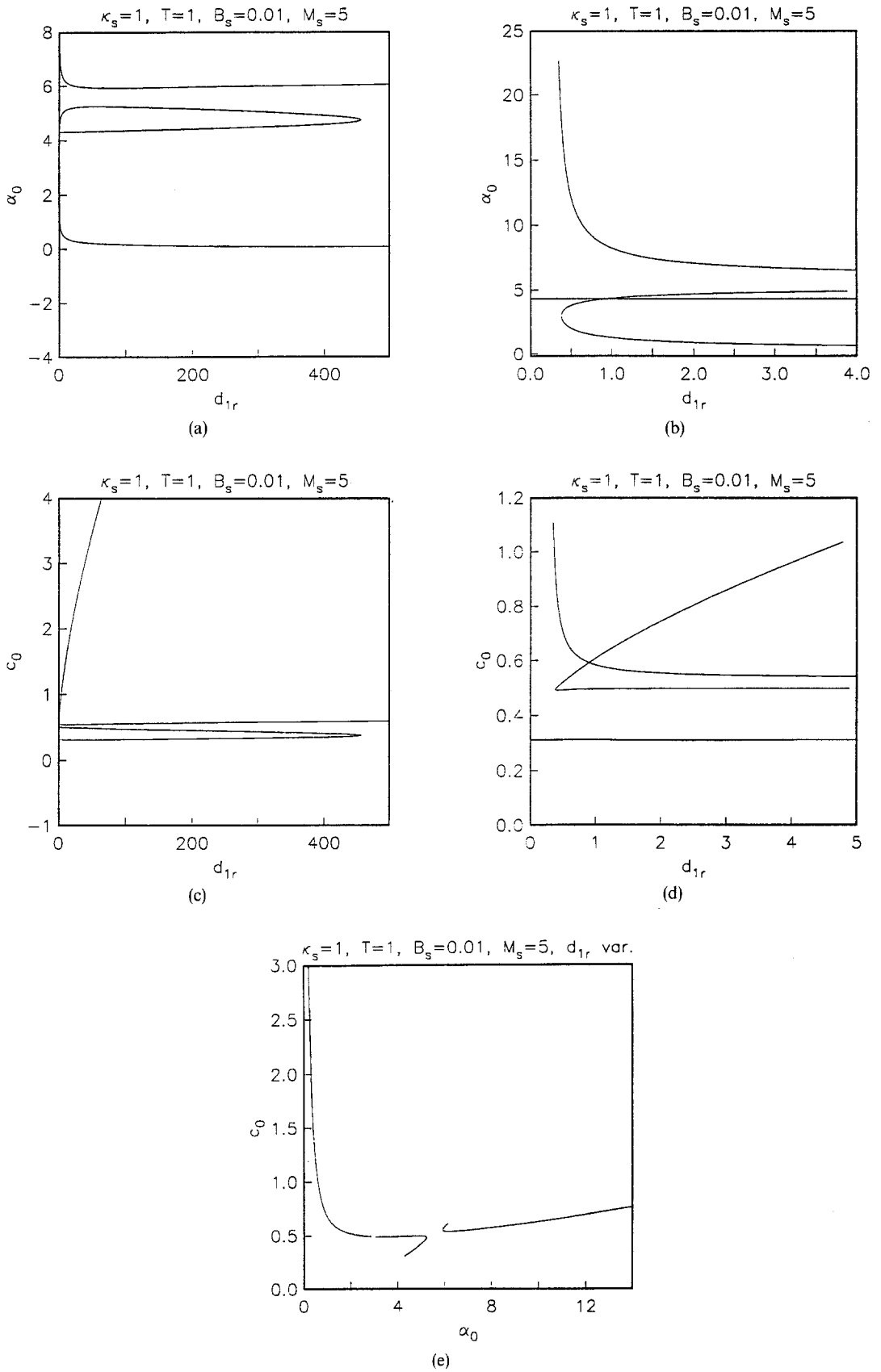

Figure 7. (a) Linear neutral α_0 against d_{1r} with $\kappa_s = 1$, $\bar{T} = 1$, $B_s = 0.01$, and $M_s = 5$. (b) Same as (a) but shown on a different scale. (c) c_0 against d_{1r}, other parameters as in (a). (d) Same as (c) but shown on a different scale. (e) α_0 against c_0 with d_{1r} varying, other parameters as in (a).

5.2. Analysis of Limiting Case for Linear Theory

The limiting cases, where some of the wall parameters become large, are of some interest and examined below. The following results are readily deduced from the relations (5.1a–d).

(i) $\kappa_s \neq 0$ and d_{1r} finite with one or more of $\bar{T}, B_s$ becoming large.

Here the only behaviour consistent with the eigenrelations is that $s_0 \to \pm\infty$ and α_0 and c_0 approaching the rigid-wall values α_{0r}, c_{0r} given by

$$c_{0r} = \frac{\alpha_{0r}^2}{2\lambda_1} I_0, \qquad \alpha_{0r} = \lambda_1 \left(\frac{4}{2\pi^2 \lambda_2^2 I_6^5} \right)^{1/11}. \tag{5.2}$$

(ii) $\bar{T} = M_s = B_s = 0$, d_{1r} finite, $\kappa_s \to \infty$.

If $\kappa_s \to +\infty$, then $s_0 = -\kappa_s \to -\infty$ and (5.1b–d) show that both c_0, α_0 remain $O(1)$ and approach their rigid-wall values.

If $\kappa_s \to -\infty$, then in addition to α_0, c_0 approaching the rigid-wall values, there is another possibility given by

$$c_0 \sim -2\kappa_s + o(1), \qquad \alpha_0 \sim 2^{-3} c_0^{-5} \left(\frac{-\lambda_{2\pi}}{\lambda_1} \right)^{-2}. \tag{5.3}$$

However, even though the limit $\kappa_s \to -\infty$ is mathematically interesting it is not possible on physical grounds and therefore we do not consider it further.

(iii) $d_{1r} \to +\infty$.

From (5.1) we find that both α_0, c_0 become large with

$$c_0 \sim \frac{\alpha_0^2 I_0}{2\lambda_1}. \tag{5.4}$$

The precise limiting form depends on the value of $\bar{T}$, M_s, and B_s. For instance, if $\bar{T} \neq 0$ and $M_s = B_s = 0$, then

$$\alpha_0 \sim \frac{I_0 d_{1r}}{8\lambda_2 \pi \bar{T}^2}.$$

If $\bar{T} \neq 0$, $Ms \neq 0$, and $B_s \neq 0$, then

$$\alpha_0 \sim \left(-\frac{2 d_{1r} \lambda_1^4}{I_0^3 \lambda_2 \pi} \right)^{1/9}.$$

If $\bar{T} = M_s = B_s = 0$ and $\kappa_s \neq 0$, then

$$\alpha_0 \sim -\frac{d_{1r}}{\lambda_2 \pi I_0}.$$

If $M_s = 0$ and $B_s \neq 0$, then

$$\alpha_0 \sim \left(\frac{-I_0 d_{1r}}{8\lambda_2 \pi B_s^2} \right)^{1/5}.$$

(iv) M_s nonzero.

This case is treated separately because of an additional mode which appears. First if $d_{1r} = 0$ and M_s becomes large, then, in addition to (5.2), there is another solution given by

$$\alpha_0 \sim \left(\frac{-2\lambda_2^2 \pi^2}{\lambda_1} \right)^{1/9} M_s^{-5/9}, \qquad c_0 \sim \frac{\lambda_1}{2 M_s \alpha_0^2}.$$

Next for M_s nonzero and $d_{1r} \to \infty$, one possibility is as given in (iii) above and (5.4). Another solution is

$$\alpha_0 \sim \left(\frac{-3\lambda_2 \pi}{2 M_s d_{1r}} \right)^{1/3}, \qquad c_0 \sim \frac{\lambda_1}{2 M_s \alpha_0^2}.$$

5.3. Nonlinear Neutral Results

In this section we examine the nonlinear equilibrium solutions of (3.10). The amplitude equation (3.10) may be written as

$$\frac{\partial(|\bar{A}|^2)}{\partial T_1}+c_g\frac{\partial(|A|^2)}{\partial X_1}=\frac{2(s_0^2+(s_0-c_0\lambda_1)^2)}{D_5 s_0(s_0-c_0\lambda_1)}|\bar{A}|^2$$
$$\times\left[\frac{\alpha_0\lambda_1^2}{\sqrt{2\bar{m}}}+\frac{\alpha_0^2c_0^3d_{1r}\lambda_1^2}{s_0^2+(s_0-c_0\lambda_1)^2}-\frac{2c_0^2\alpha_0\lambda_2}{\lambda_1(s_0^2+(s_0-c_0\lambda_1)^2)}(s_0^2\varphi_l(\gamma_c)+(s_0-c_0\lambda_1)^2\varphi_l(|\sigma|\gamma_c))\right], \quad (5.5)$$

where $\varphi_l=\text{Real}(i\varphi)$ and γ_c, σ are as given in (4.4)–(4.6).

The nonlinear equilibrium solutions of (5.5) are obtained by setting the right-hand side of (5.5) to zero and solving this in conjunction with (5.1b, c). This gives.

$$\frac{\alpha_0\lambda_1^2}{\sqrt{2\bar{m}}}+\frac{\alpha_0^2c_0^3d_{1r}\lambda_1^2}{s_0^2+(s_0-c_0\lambda_1)^2}=\frac{2c_0^2\alpha_0\lambda_2}{\lambda_1(s_0^2+(s_0-c_0\lambda_1)^2)}(s_0^2\varphi_l(\gamma_c)+(s_0-c_0\lambda_1)^2\varphi_l(|\sigma|\gamma_c)). \quad (5.6)$$

For the velocity jump across the critical layer we took the model

$$\varphi_l(\gamma_c)=-\frac{\gamma_c\pi C^{(1)}}{\gamma_c C^{(1)}+\pi},$$

which agrees well with the numerically calculated values for γ_c small or large, see also Gajjar and Smith (1985).

Some sample nonlinear results are shown in Figures 8 and 9 for different values of the compliant-wall parameters. A simple interpretation of these results is that the curves in Figure 8(a), (c) for example, represent a cut at a fixed large Reynolds number through the neutral surface in the wave number or phase speed, energy and Reynolds number space. (In place of energy we have used a scaled magnitude of the disturbance amplitude.) For a channel with rigid walls such surfaces have been computed numerically at finite Reynolds numbers by Orszag and Patera (1983) and Herbert (1977). Similar computations for a channel with compliant boundaries are presented in Rotenberry (1992) and Ehrenstein and Rossi (1993), but using a very much simplified model for the motion of the wall.

In Figure 8(a)–(f) we show the variation of the neutral wave number with neutral amplitude for the case of the simplified model in which all the wall parameters except the spring stiffness κ_s and damping d_{1r} are zero. With zero damping the results are similar to those for the rigid-wall case, Figure 8(a), (b). With nonzero values of damping, and large κ_s, the curves increase up to a peak amplitude and then terminate at a slightly lower finite amplitude, Figure 8(a), (c). With a nonzero value of damping and small κ_s there are multiple roots even for the linear case. Two of the roots connect together as the nonlinear amplitude increases, see Figure 8(c), (d). The third root also terminates at some finite amplitude, Figure (8d).

With the scaled tension $\bar{T}$ nonzero, the nonlinear results differ considerably from the rigid-wall case when the damping is nonzero. There are again multiple roots to the dispersion curves with $d_{1r}\neq 0$. In Figure 9 it is seen that two of the roots connect together nonlinearly. The third root has the wave number increasing, but with the amplitude decreasing, as problem (4.4) becomes strongly nonlinear.

The behaviour of the neutral surfaces when some of the other parameters are varied is much more complicated, and further results are not presented here. Some of properties of these solutions may be deduced from the analysis of the limiting cases below.

The properties of the nonlinear neutral results in the limit as γ_c tends to zero is examined next. The results given below can be obtained as in Smith and Bodonyi (1982). We consider the various possibilities in turn.

(v) $\bar{T}=M_s=B_s=0$ and $\kappa_s\neq 0$.

First if $d_{1r}=0$, then the dispersion relations show that

$$\alpha_0\sim\alpha_{01}\gamma_c^{-2/5}, \qquad \bar{A}\sim a_{01}\gamma_c^{-2/5}, \qquad c_0\sim\alpha_0^2 I_0\lambda_1, \quad (5.7)$$

where

$$\alpha_{01}=2^{-3/5}(-\lambda_2C^{(1)}I_0)^{-2/5}|\kappa_s|^{-3/5}\lambda_1^{7/5}, \qquad a_{01}=\left(\frac{\lambda_1^2}{2^{3/2}\alpha_{01}}\right)^{2/3}\frac{1}{|\kappa_s|}. \quad (5.8)$$

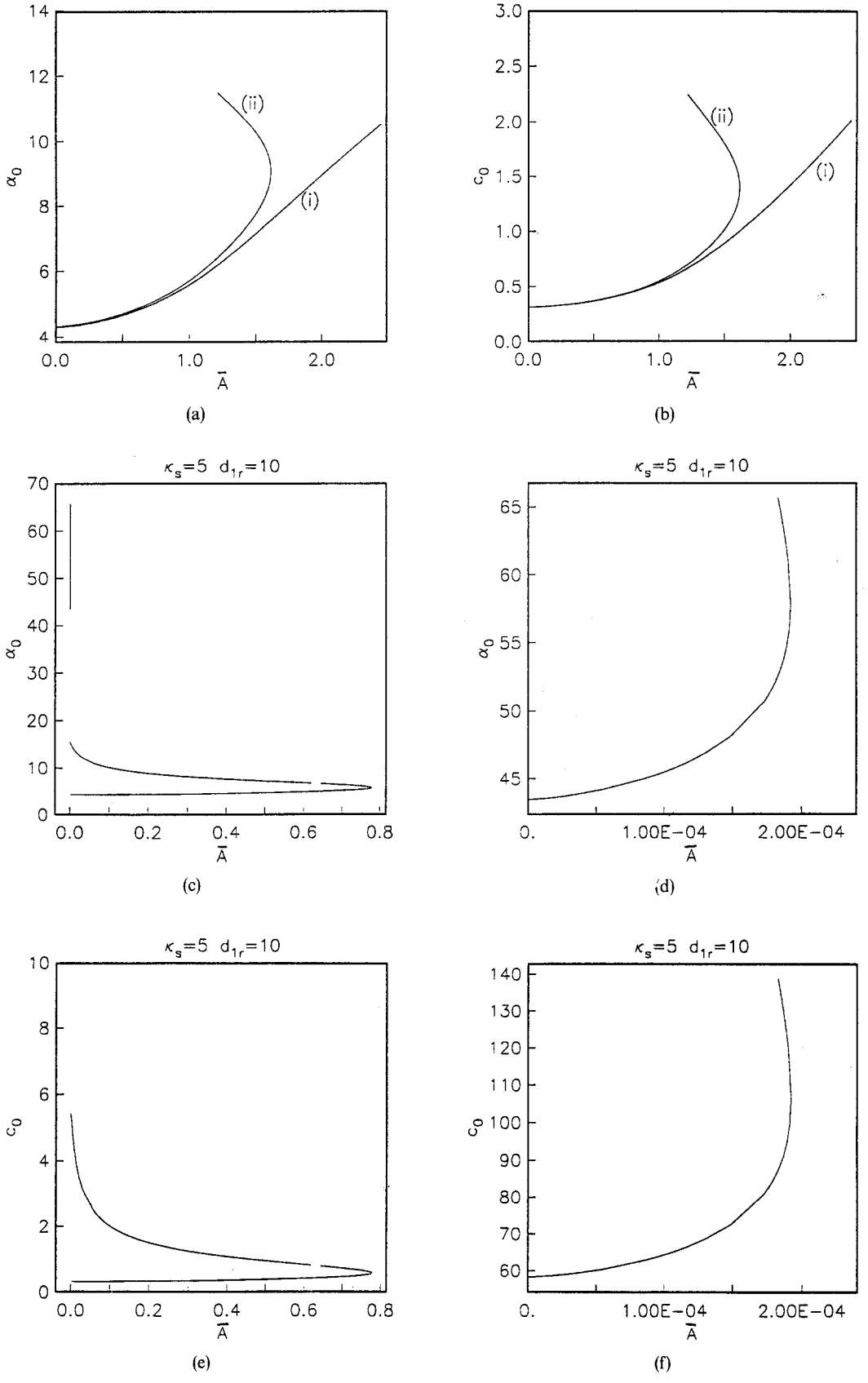

Figure 8. (a) Nonlinear neutral amplitudes $\bar{A}$ against wave number α_0. $\bar{T} = M_s = B_s = 0$. Curve (i) has $\kappa_s = 10$ and $d_{1r} = 0$, and curve (ii) has $\kappa_s = 50$ and $d_{1r} = 10$. (b) same as (a) except for phase speed c_0. (c) Nonlinear neutral amplitude $\bar{A}$ against α_0 with $\kappa_s = 5$, $d_{1r} = 10$, and the other parameters as in (a). (d) Same as (c) but shown on a different scale. (e) Same as (c) but for phase speed c_0. (f) Same as (e) but shown on a different scale.

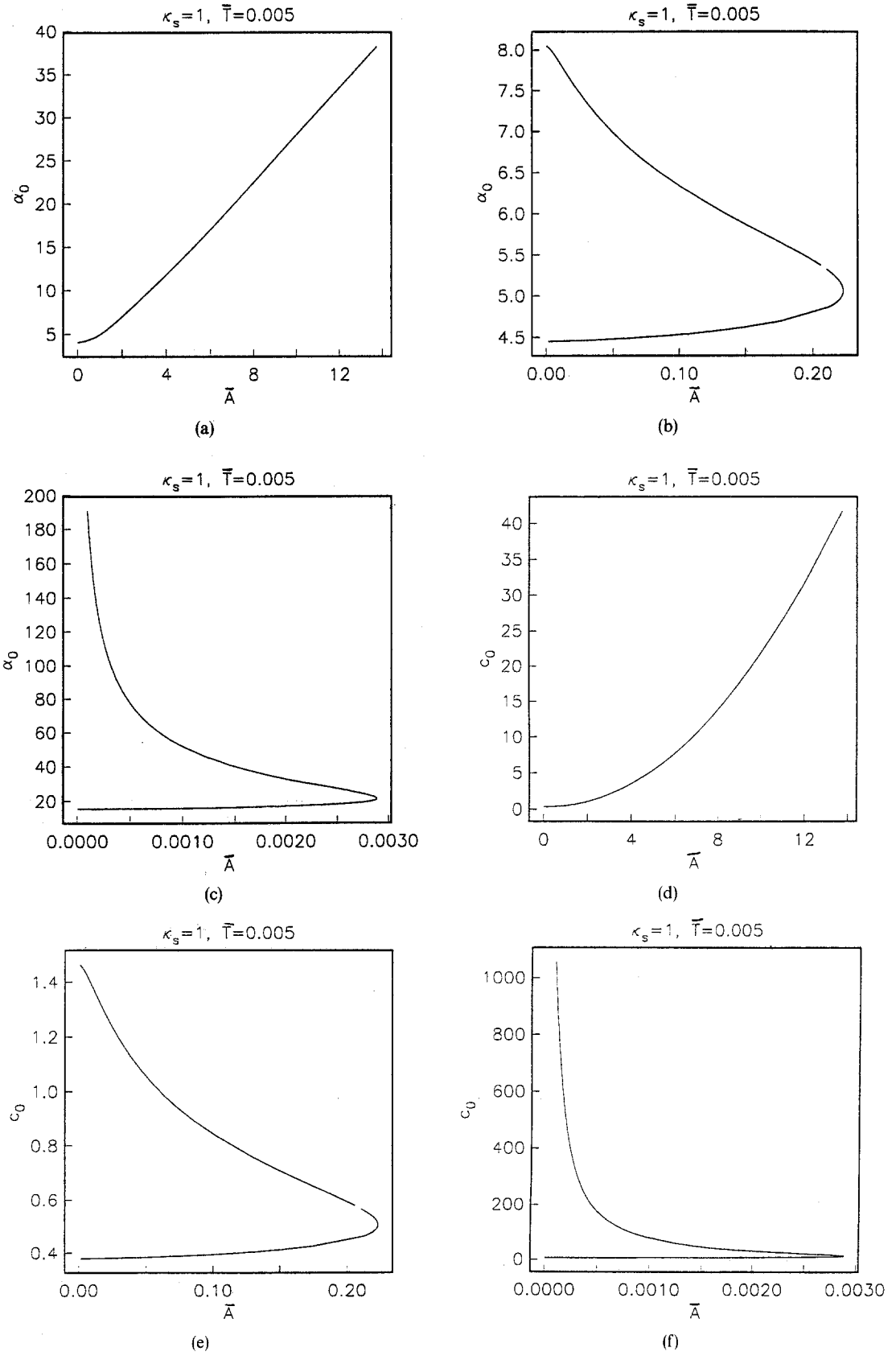

Figure 9. (a) Nonlinear neutral amplitude $\bar{A}$ against wave speed α_0, with $\kappa_s = 1$, $\bar{T} = 0.005$, $M_s = B_s = 0$, and $d_{1r} = 0$. (b) Same as (a) but with $d_{1r} = 5$. (c) Same as (b) but showing the third root. (d) Same as (a) but for phase speed c_0. (e) and (f) Same as (b) and (c) but for phase speed c_0.

If $d_{1r} \neq 0$ there are no consistent balances with any of the terms in the dispersion relations and this suggests that the solutions must terminate at some finite values of γ_c as indicated by the numerical solutions.

(vi) $\bar{T} \neq 0$ and $M_s = B_s = 0$.

With $d_{1r} = 0$ it is found that

$$\alpha_0 \sim \alpha_{02}\gamma_c^{-2/11}, \qquad \bar{A} \sim a_{02}\gamma_c^{-2/11}, \qquad c \sim \frac{\alpha_0^2 I_0}{2\lambda_1}, \tag{5.9}$$

with

$$\alpha_{02} = \alpha_{0r}\left(\frac{\pi^2}{C^{(1)2}(d_{10}+d_{20})^2}\right)^{1/11}, \qquad a_{02} = \frac{\lambda_1^{4/3}}{2\alpha_{02}^{8/3}}\left|\frac{\bar{T}+I_0/2}{\bar{T}}\right|^{3/2},$$

and where

$$d_{10} = \frac{\bar{T}^2}{\bar{T}^2+(\bar{T}+I_0/2)^2}, \qquad d_{20} = (1-d_{10})\left|\frac{\bar{T}}{\bar{T}+I_0/2}\right|^{3/2}.$$

With damping present ($d_{1r} \neq 0$) the limiting behaviour is very different and we find that

$$\alpha_0 \sim \alpha_{03}\gamma_c^{-1}, \qquad \bar{A} \sim a_{03}\gamma_c^2, \tag{5.10}$$

and

$$\alpha_{03} = -\frac{d_{1r}\lambda_1^2 I_0}{(\bar{T}^2+(\bar{T}+I_0/2)^2)4\lambda_2 C^{(1)}(d_{10}+d_{20})}.$$

The constant a_{03} is of the same form as a_{02} with α_{02} replaced by α_{03}.

Whereas without damping the amplitude increases indefinitely, with damping the amplitude goes to zero as γ_c goes to zero.

(vii) $M_s = 0$ and $B_s \neq 0$.

With $d_{1r} = 0$ this is the same as the rigid case given by

$$\alpha_0 \sim \alpha_{04}\gamma_c^{-2/11}, \qquad \bar{A} \sim a_{04}\gamma_c^{-2/11}, \qquad c \sim \frac{\alpha_0^2 I_0}{2\lambda_1}, \tag{5.11}$$

and

$$\alpha_{04} = \alpha_{0r}\left(\frac{\pi^2}{C^{(1)2}}\right)^{1/11}, \qquad a_{04} = \lambda_1^{7/3}\alpha_{04}^{-4/3}I_0^{-1}\gamma_c^{-2/11}.$$

With damping present the corresponding behaviour is

$$\alpha_0 \sim \alpha_{05}\gamma_c^{-1/5}, \qquad \bar{A} \sim a_{05}\gamma_c^{-2/15}, \tag{5.12}$$

and

$$\alpha_{05} = \left(\frac{-8\lambda_2 C^{(1)}B_s^2}{\lambda_1^2 d_{1r} I_0}\right)^{-1/5},$$

with a_{05} of the same form as a_{04} but with α_{04} replaced by α_{05}

(viii) $M_s \neq 0$.

Here there are two modes with one mode behaving exactly as in the rigid case given by (5.11). The other mode has a different behaviour depending on whether d_{1r} is zero or not. If the damping is zero, then

$$\alpha_0 \sim \alpha_{05}\gamma_c^{2/9}, \qquad \bar{A} \sim a_{05}\gamma_c^{-10/27}, \qquad c_0 = \frac{\lambda_1}{2M_s\alpha_0^2},$$

where

$$\alpha_{05} = \left(\frac{2^6\lambda_1 M_s^5}{\lambda_2^2 C^{(1)2}}\right)^{-1/9}, \qquad a_{05} = \lambda_1^3 M_s \alpha_{05}^{4/3}.$$

If $d_{1r} \neq 0$, then

$$\alpha_0 \sim \alpha_{06}\gamma_c^{1/3}, \qquad \bar{A} \sim \lambda_1^3 M_s \alpha_{06}^{4/3}\gamma_c^{-9/2}, \qquad c_0 = \frac{2\lambda_1}{M_s\alpha_0^2},$$

and

$$\alpha_{06} = \left(\frac{-\lambda_2 C^{(1)}}{2\lambda_1^4 M_s d_{1r}}\right)^{1/3}.$$

The numerical results shown in Figures 8 and 9 are in good agreement with the predictions above.

5.4. Further Properties of the Amplitude Equation

Introducing the variable $T = T_1 - c_g X_1$, (3.10) may be expressed as

$$\frac{d|\bar{A}|^2}{dT} = k_0 k_1 \left[1 - \frac{k_2}{k_1}(d_1\varphi_l(\gamma_c) + d_2\varphi_l(|\sigma|\gamma_c))\right]|\bar{A}|^2, \tag{5.13}$$

where the constants k_0, k_1, k_2, d_0, and d_1 are given by

$$k_0 = \frac{2(s_0^2 + (s_0 - c_0\lambda_1)^2)}{\{-2M_s\lambda_1^2\alpha_0^2c_0^3 + (s_0 - c_0\lambda_1)(2c_0\lambda_1\hat{\lambda}_1 - s_0(\hat{\lambda}_1 - \lambda_1) + \alpha_0^2 I_0\lambda_1)\}}, \tag{5.14a}$$

$$k_1 = \frac{\alpha_0\lambda_1^2}{\sqrt{2\bar{m}}} + \frac{\alpha_0^2 c_0^3 d_{1r}\lambda_1^2}{s_0^2 + (s_0 - c_0\lambda_1)^2}, \tag{5.14b}$$

$$k_2 = \frac{2c_0^2\alpha_0\lambda_2}{\lambda_1}, \tag{5.14c}$$

and

$$d_1 = \frac{s_0^2}{s_0^2 + (s_0 - c_0\lambda_1)^2}, \qquad d_2 = 1 - d_1.$$

Note that k_1, d_1, and d_2 are positive whilst k_2 and φ_l are negative. The nonlinear term thus exerts a stabilizing/destabilizing influence depending on whether k_0 is positive or negative. The linear growth rate

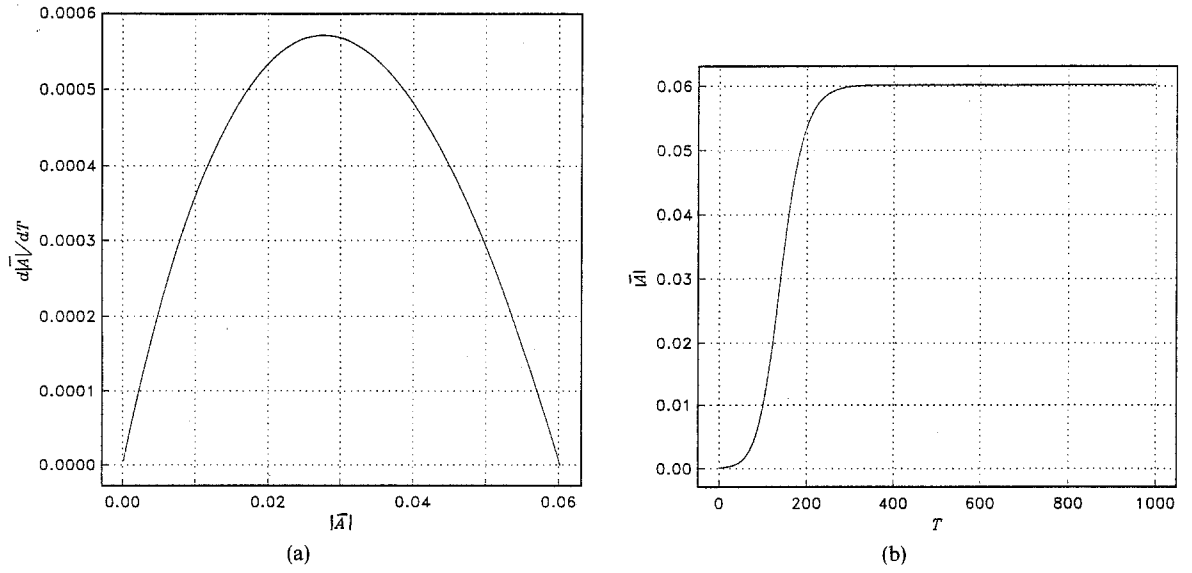

Figure 10. (a) Phase diagram of (5.13) with $\kappa_s = 1$, $d_{1r} = 0$, $B_s = 0.0001$, $\bar{T} = 1$, $M_s = 117.83$, $\alpha_0 = 4.031$, and $c_0 = 0.3316$ giving $k_0 = -0.3147$, $k_1 = 2.4655$, $k_2 = -0.8864$, and $d_1 = 0.6679$. (b) Numerical solution of (5.13) with parameters as in (a).

is $k_0(k_1 + k_2\pi)$. The right-hand side of (5.13) may be expressed as

$$k_0[k_1 + k_2\pi]|\bar{A}|^2 - k_0k_2[\pi + d_1\varphi_l(\gamma_c) + d_2\varphi_l(|\sigma|\gamma_c)]|\bar{A}|^2.$$

For an unstable wave the first bracketed term is positive and the second bracketed term is zero. As the amplitude increases, if k_0 is negative, then the second term causes a reduction in the growth rate which eventually crosses zero, see Figure 10(a). This suggests that solutions of (5.13) starting from a lineary unstable state, with k_0 negative, must reach a finite amplitude at large times T.

We consider next the stability of the equilibrium solutions of (5.13). Let $|\bar{A}|^2 = |A_e|^2 + \tilde{B}$ where $\tilde{B} \ll 1$ and the suffix e denotes an equilibrium value. Then substituting into (5.13) and linearizing gives

$$\frac{d\tilde{B}}{dT} = -k_0k_2(d_1\varphi_l'(\gamma_{ce}) + d_2|\sigma|\varphi_l'(|\sigma|\gamma_{ce}))|A_e|^2\left(\frac{d\gamma_c}{d|\bar{A}|^2}\right)_e\tilde{B}. \tag{5.15}$$

Thus if k_0 is positive the equilibrium amplitudes are unstable whereas if k_0 is negative the equilibrium amplitudes are stable. For the rigid-wall case (and the accelerating boundary layer) described in Gajjar and Smith (1985), k_0 is positive confirming the tentative suggestions of Gajjar and Smith (1985) that the equilibrium amplitude solutions in these flows are unstable. For the compliant-wall case there are several parameter regimes where k_0 can take both signs. An an example in Figure 10(b) we show the numerical solution to (5.13) for an unstable wave, with the wall parameters such that k_0 is negative, which attains a stable finite equilibrium amplitude as predicted above.

6. Summary

In this paper we have developed a self-consistent theory to study the effect of compliance on the hydrodynamic stability of flow in a channel. We have established an analytic procedure for the analysis of channel flow with compliant boundaries which is a counterpart to the well-known theory for channel flows with rigid boundaries.

An amplitude equation governing the nonlinear evolution of disturbances to the basic flow has been derived and solutions obtained for both the linear and nonlinear theories.

A few important conclusions which may be drawn from the present work are as follows. Firstly our results show that the use of Hooke's Law alone (with $\bar{T}$, M_s, B_s, and damping all set to zero) gives results which are markedly different from the ones in which some of these parameter values are not zero. This suggests that the use of Hooke's Law alone can lead to misleading results for a real compliant surface. The computations of Rotenberry (1992) and Ehrenstein and Rossi (1993) are based on such a simplified model of the motion of the wall. The most pronounced deviations from the rigid-wall results arise with nonzero values of the mass stiffness parameter M_s, viscoelastic wall damping parameter $\bar{d}$, and small values of tension. The effect of increased wall damping is destablizing on TSI in agreement with similar observations in the boundary-layer flow over compliant surfaces, see Carpenter (1990).

Many of the limiting cases analysed in Section 5 point to the importance of a new Rayleigh structure for the flow with enhanced phase speeds and shorter waves. For example from (5.11) it is seen that as α_0 formally increases to $O(\varepsilon^{-1})$ the unscaled wave number α and phase speed c both become $O(1)$. This and other new structures predicted in Section 5 are currently being investigated. One important result which may be deduced is that the basic plane Poiseuille flow with a compliant surface will be linearly unstable to Rayleigh waves. Similar conclusions may also be drawn for the case of a circular pipe with a flexible wall in which the basic state is taken to be the Hagen–Poiseuille flow and where the motion of the boundary is governed by a similar model to the one used here. This short wavelength inviscid instability is related to the travelling-wave flutter instability which has been observed in some medical experiments. Some aspects of this have already been investigated in the context of some physiological phenomena, as mentioned in the Introduction, see Grotberg (1994). However, the importance of this instability suggests that a more systematic and rational investigation is clearly desirable and this is also being considered.

Finally, one other important finding is that for the flow studied here a range of parameter values exists for which the nonlinear equilibrium amplitudes emanating from the Haberman viscous critical layer are stable. This is in sharp contrast to that for the rigid-wall case and for many other related boundary-layer flows.

Acknowledgement

The referees are thanked for their comments.

Appendix A

The constants D_0–D_5 and the integrals appearing in the text are defined as follows:

$$I_0 = \int_0^1 U_B^2\, dy,$$

$$I_1 = \int_0^1 U_B\, dy,$$

$$I_2 = \int_0^1 U_B^2 \int_{1/2}^{y_1} \frac{1}{U_B^2}\, dy_1\, dy,$$

$$I_3 = \int_0^1 U_B^2 \int_{1/2}^{y} \frac{1}{U_B^2} \int_0^{y_1} U_B^2\, dy_2\, dy_1\, dy,$$

$$I_4 = \int_{1/2}^0 \left(\frac{1}{U_B^2} - \frac{1}{\lambda_1^2 y^2} + \frac{2\lambda_2}{\lambda_1^3 y} \right) dy,$$

$$I_5 = \int_{1/2}^0 \frac{1}{U_B^2} \int_0^y U_B^2\, dy_1\, dy,$$

$$I_6 = \int_{1/2}^1 \left(\frac{1}{U_B^2} - \frac{1}{\hat{\lambda}_1^2 (y-1)^2} + \frac{2\hat{\lambda}_2}{\hat{\lambda}_1^3 (y-1)} \right) dy,$$

$$I_7 = \int_{1/2}^1 \frac{1}{U_B^2} \int_1^y U_B^2\, dy_1\, dy,$$

$$D_0 = \alpha_0 \lambda_1 \left[\frac{s_0 \lambda_1 c_0}{(s_0 - c_0 \lambda_1)} \left(I_4 + \frac{2}{\lambda_1^2} \right) - \alpha_0^2 I_5 \right] - \frac{\alpha_0 \lambda_2}{\lambda_1^2} \frac{s_0 \lambda_1 c_0}{(s_0 - c_0 \lambda_1)} - \frac{2\lambda_2 \alpha_0 c_0}{\lambda_1},$$

$$D_1 = \frac{2\lambda_2 \alpha_0 c_0^2}{\lambda_1^2} \left(\frac{\lambda_1 c_0}{s_0 - c_0 \lambda_1} \right) \left(1 + \ln \left| \frac{c_0}{\lambda_1} \right| \right) + \frac{2\lambda_2 \alpha_0 c_0^2}{\lambda_1^2} \ln \left| \frac{c_0}{\lambda_1} \right|,$$

$$D_2 = \alpha_0 \hat{\lambda}_1 \left[c_0 \hat{\lambda}_1 \left(I_6 - \frac{2}{\hat{\lambda}_1^2} \right) - \alpha_0^2 I_7 \right] - \frac{2\hat{\lambda}_2 \alpha_0 c_0}{\hat{\lambda}_1} + \frac{\alpha_0 \hat{\lambda}_2 c_0}{\hat{\lambda}_1},$$

$$D_3 = c_0 D_2 + \alpha_0 \left[2\alpha_0^2 c_0 I_1 + \alpha_0^2 I_2 \left(\frac{s_0 c_0 \lambda_1}{(s_0 - c_0 \lambda_1)} \right) - \alpha_0^4 I_3 \right] - \frac{2\hat{\lambda}_2 \alpha_0 c_0^2}{\hat{\lambda}_1} \ln \left| \frac{c_0}{\hat{\lambda}_1} \right|,$$

$$D_4 = c_0 D_0 + \lambda_1 D_1 + D_3 \left(1 - \frac{c_0 \lambda_1}{s_0} \right),$$

$$D_5 = \left[-\frac{2M_s \lambda_1^2 \alpha_0^2 c_0^3}{(s_0 - c_0 \lambda_1)} + 2c_0 \lambda_1 \hat{\lambda}_1 - s_0 (\hat{\lambda}_1 - \lambda_1) + \alpha_0^2 I_0 \lambda_1 \right] \frac{1}{s_0}.$$

References

Benjamin, T.B. (1960) Effects of a flexible boundary on hydrodynamic stability. *J. Fluid Mech.*, **9**, 513–532.

Benjamin, T.B. (1963). The threefold classification of unstable disturbances in flexible surfaces bonding inviscid flows. *J. Fluid. Mech.*, **16**, 436–450.

Brown, P.G., Brown, S.N., Smith, F.T., and Timoshin, S.N. (1993). On the starting process of strongly nonlinear vortex/Rayleigh-wave interactions. *Mathematika*, **40**, 7–29.

Bushnell, D.M., Heffner, J.N., and Ash, R.L. (1977). Effects of compliant wall motion on turbulent boundary layer. *J. Phys. Fluids*, **20**, 531–548.

Carpenter, P.W. (1990). Status of transition delay using compliant walls. *Viscous Drag Reduction in Boundary Layers* (ed. D.M. Bushnell and J.N. Heffner), pp. 79–113. AIAA, New York.

Carpenter, P.W., and Gajjar, J.S.B. (1990). A general theory for two- and three-dimensional wall-mode instabilities in boundary layer over isotropic and anisotropic compliant walls. *Theoret. Comput. Fluid Dynamics*, **1**, 349–378.

Carpenter, P.W., and Garrad, A.D. (1985). The hydrodynamic stability of flow over Kramer-type compliant surfaces. Part 1. Tollmien–Schlichting instabilities. *J. Fluid Mech.*, **155**, 465–510.

Carpenter, P.W., and Garrad, A.D. (1986). The hydrodynamic stability of flow over Kramer-type compliant surfaces. Part 2. Flow-induced surface instabilities. *J. Fluid Mech.*, **170**, 199–232.

Ehrenstein, U., and Rossi, M. (1993). Nonlinear Tollmien–Schlichting waves for plane Poiseuille Flow with a compliant wall. *European J. Mech. B–Fluids*, **12**(6), 789–810.

Gajjar, J.S.B. (1996). Nonlinear stability of cross-flow vortices in compressible boundary layers. *Stud. Appl. Math.*, in press.

Gajjar, J.S.B., and Smith, F.T. (1985). On the global instability of free disturbances with time-dependent nonlinear viscous critical layers. *J. Fluid Mech.*, **157**, 53–77.

Gavriely, N., Palti, Y., Alroy, G., and Grotberg, J.B. (1984). Measurements and theory of wheezing breath sounds. *J. Appl. Physiol.*, **57**, 481–492.

Gavriely, N., Shee, T.R., Cugell, D.W., and Grotberg, J.B. (1989). Flutter in flow limited collapsible tubes: a mechanism for generation of wheezes. *J. Appl. Physiol.*, **66**, 2251–2261.

Grotberg, J.B. (1994). Pulmonary flow and transport phenomena. *Ann. Rev. Fluid Mech.*, **26**, 529–571.

Grotberg, J.B., and Davies, S.H. (1980). Fluid dynamic flapping of a collapsible channel: sound generation and flow limitation. *J.Biomech.*, **13**, 219–230.

Grotberg, J.B., and Reiss, E.L. (1984). Subsonic flapping flutter. *J. Sound Vibration*, **92**, 349–361.

Grotberg, J.B., and Shee, T.R. (1985). Compressible-flow channel flutter. *J. Fluid Mech.*, **159**, 175–193.

Gyorgyfalvy, D. (1967). Possibilities of drag reduction by the use of flexible skin. *J. Aircraft*, **4**, 186–192.

Haberman, R. (1972). Critical layers in parallel flows. *Stud. Appl. Math.*, **51**, 139–161.

Hains, F.D., and Price, J.F. (1962). Effect of a flexible wall on the stability of Poiseuille flow. *J. Phys. Fluids*, **5**(3), 365.

Herbert, T. (1977). Finite amplitude stability of plane parallel flows. AGARD CP-224, 3/1–10.

Landahl, M.T. (1962). On the stability of a laminar incompressible boundary layer over a flexible surface. *J. Fluid. Mech.*, **13**, 609–632.

Landahl, M.T., and Kaplan, R.E. (1965). Effect of compliant walls on boundary layer stability and transition. *AGARD*, **97**, 1–353.

Orszag, S., and Patera, A. (1983). Secondary instability of wall-bounded shear flows. *J. Fluid Mech.*, **128**, 347–385.

Reid, W.H. (1965). In *Basic Developments in Fluid Dynamics*, vol. 1 (ed. M. Holt). Academic Press, New York.

Riley, J.J., Gad-el-Hak, M., and Metcalfe, R.W. (1988). Compliant coatings. *Ann. Rev. Fluid Mech.*, **20**, 393–420.

Rotenberry, J.M. (1992). Finite-amplitude shear waves in channel compliant boundaries. *Phys. Fluids A*, **4**(2), 270–276.

Rotenberry, J.M., and Saffman, P.G. (1990). Effect of compliant boundaries on weakly nonlinear shear waves in channel flow. *SIAM J. Appl. Math.*, **50**(2), 361–394.

Smith, F.T. (1979). Instability of flow through pipes of general cross section (part 2).*Mathematika*, **26**, 211–223.

Smith, F.T., and Bodonyi, R.J. (1982). Nonlinear critical layers and their development in streaming-flow stability. *J. Fluid Mech.*, **118**, 165–185.

Willis, G.J.K. (1986). Hydrodynamic stability of boundary layer over compliant surfaces. Ph.D Thesis, University of Exeter.

Wu, X., Stewart, P.A., and Cowley, S.J. (1996). On the weakly non-linear fully coupled resonant triad interactions in the Blasius boundary layer. *J. Fluid Mech.*, to appear.